The Tropospheric Biennial Oscillation and Asian–Australian Monsoon Rainfall

GERALD A. MEEHL AND JULIE M. ARBLASTER

National Center for Atmospheric Research, Boulder, Colorado*

(Manuscript received 16 January 2001, in final form 26 September 2001)

ABSTRACT

In the context of the Asian–Australian monsoon, the tropospheric biennial oscillation (TBO) is defined as the tendency for a relatively strong monsoon to be followed by a relatively weak one, and vice versa. Therefore the TBO is not so much an oscillation, but a tendency for the system to flip-flop back and forth from year to year. The more of these interannual flip-flops or transitions, the more biennial the system. The transitions occur in northern spring for the south Asian or Indian monsoon and in northern fall for the Australian monsoon involving coupled land–atmosphere–ocean processes over a large area of the Indo-Pacific region. There is considerable seasonal persistence from the south Asian to Australian monsoon as noted in previous studies, with a strong south Asian or Indian monsoon tending to precede a strong Australian monsoon and vice versa for weak monsoons. Therefore, transitions from March–May (MAM) to June–September (JJAS) tend to set the system for the next year, with a transition to the opposite sign the following year. Quantifying the role of the conditions that contribute to these transitions in the TBO and their relationship to ENSO is crucial for verifying their accurate representation in models, which should lead to improved seasonal forecast skill. An analysis of observed data shows that the TBO (with roughly a 2–3-yr period) encompasses most ENSO years (with their well-known biennial tendency) as well as additional years that contribute to biennial transitions. Thus the TBO is a fundamental feature of the coupled climate system over the entire Indian–Pacific region. El Niño and La Niña events as well as Indian Ocean SST dipole events are large amplitude excursions of the TBO in the tropical Pacific and Indian Oceans, respectively, associated with coupled ocean dynamics, upper-ocean temperature anomalies, and associated ocean heat content anomalies. Conditions postulated to contribute to TBO transitions involve anomalous Asian land surface temperatures, Pacific and Indian Ocean SST anomalies, and the associated strength of the convective maximum over Australasia. These interannual transition conditions are quantified from singular value decomposition (SVD) analyses on a year-by-year basis using single and cumulative anomaly pattern correlations. This technique takes into account intermittent influences and secular variations in the strength of any particular association in any given year. Anomalous Pacific and Indian Ocean SSTs are the dominant transition conditions in the TBO, with anomalous meridional temperature gradients over Asia a secondary factor. There is an intrinsic coupling of the anomalous strength of the convective maximum in the seasonal cycle over Australasia, surface wind forcing, ocean dynamical response, and associated SST anomalies that feed back to the strength of the convective maximum, and so on. All are tied together by the large-scale east–west circulation, the eastern and western Walker cells, in the atmosphere. By omitting El Niño and La Niña onset years from the analysis, there are similar but lower-amplitude relationships among the transition conditions and Asian–Australian monsoon rainfall. An SST transition in the Pacific is started by surface wind anomalies in the far western equatorial Pacific associated with the Australian monsoon, while an SST transition in the Indian Ocean is started by surface wind anomalies in the western equatorial Indian Ocean associated with the Indian monsoon. This provides successive forcing and response among Indian and Pacific SSTs and the Asian–Australian monsoons half a year apart. The consequent feedback to the monsoon circulations by the SST anomalies results in the TBO.

1. Introduction

The attribution of the strength of associations of conditions prior to the Asian–Australian monsoon with subsequent anomalous patterns of monsoon rainfall is one of the fundamental human and scientific problems facing the climate research community today. This is of primary importance to the economies of dozens of countries and the livelihoods of millions of people in the monsoon regions stretching from Africa, across Asia to the Pacific. To accurately represent coupled processes in the climate system in forecast models, we must first identify and quantify such processes in the observed system.

The tropospheric biennial oscillation (TBO) is defined here as the tendency for a relatively strong monsoon to

* The National Center for Atmospheric Research is sponsored by the National Science Foundation.

Corresponding author address: Dr. Gerald A. Meehl, Climate and Global Dynamics Division, National Center for Atmospheric Research, P.O. Box 3000, Boulder, CO 80307.
E-mail: meehl@ncar.ucar.edu

be followed by a relatively weak one, and vice versa, with the transitions occurring in the season prior to the monsoon involving coupled land–atmosphere–ocean processes over a large area of the Indo-Pacific region (Meehl 1997). Thus the TBO is more a tendency for the system to flip-flop back and forth from year to year, and not so much an oscillation. The more of these interannual flip-flops or transitions, the more biennial the system.

The TBO has become recognized as a candidate for understanding some of the processes that can contribute to interannual variability of a variety of parameters in the Indian and Pacific regions in both observations (Ropelewski et al. 1992; Yang et al. 1996; Yasunari 1990; Yasunari and Seki 1992; Tomita and Yasunari 1996; Meehl 1987, 1997; Meehl and Arblaster 2001b, hereafter MEAR2) and models (Ogasawara et al. 1999; Chang and Li 2000). Though there are some alternative explanations concerning how the TBO can arise (e.g., Jin et al. 1994; Goswami 1995), certain deterministic processes have been postulated to produce the TBO (Clarke et al. 1998; Chang and Li 2000; Meehl 1987, 1993, 1994, 1997; MEAR2). One of the difficulties of these TBO studies has been quantifying the contribution of various proposed mechanisms. The purpose of this paper is to address this issue, and attempt to quantify the year-to-year contributions of conditions associated with TBO transitions to patterns of Asian–Australian monsoon rainfall. We will address two questions: 1) What makes the TBO transition or ''flip-flop'' from year to year, and 2) why is northern spring March–May (MAM) particularly important for TBO transitions?

In regards to the first question, we hypothesize that certain conditions in the seasons prior to the monsoon, set up by coupled interactions in the preceding year, will cause the monsoon to be relatively stronger (or weaker) than the previous or following years, thus introducing a biennial component in spectra of area-averaged monsoon rainfall. These conditions include anomalous SSTs in the Indian and Pacific Oceans for both the south Asian and Australian monsoons, in addition to anomalous meridional temperature gradients over Asia prior to the Indian monsoon, and anomalous strength of the convective maximum prior to the Australian monsoon.

With respect to the second question, we hypothesize that the strength of the Australian monsoon, itself set up by conditions from the previous year, produces anomalous wind forcing in the western equatorial Pacific. This in turn results in an ocean dynamical response that causes tropical Pacific SST anomalies to change sign or transition, which then can affect the subsequent Indian monsoon via the large-scale east–west atmospheric circulation. More details in regards to these hypotheses will be provided below (e.g., in the discussion of Fig. 3).

Though there are a number of different types of ENSO events with protracted episodes that would weaken biennial signals (Allan and D'Arrigo 1999; Reason et al. 2000), enough ENSO events have inherent biennial tendencies so that a well-known biennial signature, with opposite sign precipitation and temperature anomalies the previous and following years, shows up in composite El Niño and La Niña events over a wide domain covering the tropical Indian and Pacific regions (e.g., Kiladis and van Loon 1988; Kiladis and Diaz 1989). Therefore, the TBO clearly must encompass this biennial tendency of ENSO. However, it has been shown that other years display similar patterns to ENSO in this large region (Meehl 1987; Lau and Wu 2001). In fact, TBO and ENSO signal strength is closer in magnitude over the Indian Ocean than the equatorial Pacific (Reason et al. 2000). Therefore the TBO must include most ENSO (El Niño and La Niña) years and some other years as well. Yet it has been difficult to quantify the various processes and conditions associated with this biennial tendency of monsoon–ENSO interaction and the additional non-ENSO years that contribute to the TBO (Webster et al. 1998). It has been argued that, of the wide array of conditions that could contribute to monsoon transitions in the TBO, most ultimately relate to anomalous surface temperature over south Asia and the tropical Indian and Pacific Oceans (Meehl 1997). It is the purpose of this paper to quantify the contributions from such anomalous surface conditions involved with a transition from relatively weak (strong) to relatively strong (weak) monsoon in consecutive years that contribute to the TBO.

To illustrate how a biennial tendency can arise in the time series of the annually recurring Asian–Australian monsoons, we show time series of area-averaged precipitation for the Indian monsoon (JJAS, 1979–99, 5°–40°N, 60°–100°E, Fig. 1a) and the Australian monsoon (DJF, 1979–99, 20°S–5°N, 100°–150°E, Fig. 1b). Solid dots indicate monsoon rainfall relatively greater (or less) than the preceding or following years. That is, if P_i is the value of area-averaged monsoon season precipitation for a given year i, then a relatively strong monsoon is defined as

$$P_{i-1} < P_i > P_{i+1}$$

and a relatively weak monsoon is defined as

$$P_{i-1} > P_i < P_{i+1}.$$

For the Indian monsoon, 13 out of 21 yr are ''biennial'' defined in that way, and 11 out of 21 yr for the Australian monsoon. El Niño and La Niña onset years correspond to some of those TBO years but not all. This was first noted by Meehl (1987). The spectra of the time series in Fig. 1a shows a peak in the TBO period of 2.6 yr with little ENSO peak for this time period in Fig. 2a (the relative power of ENSO and TBO vary over time, e.g., Webster et al. 1998). Since there is the possibility of aliasing with the annual data (Madden and Jones 2001), spectra of the monthly anomalies (including all 12 months each year) for the Indian monsoon region are shown in Fig. 2b. A similar significant TBO peak

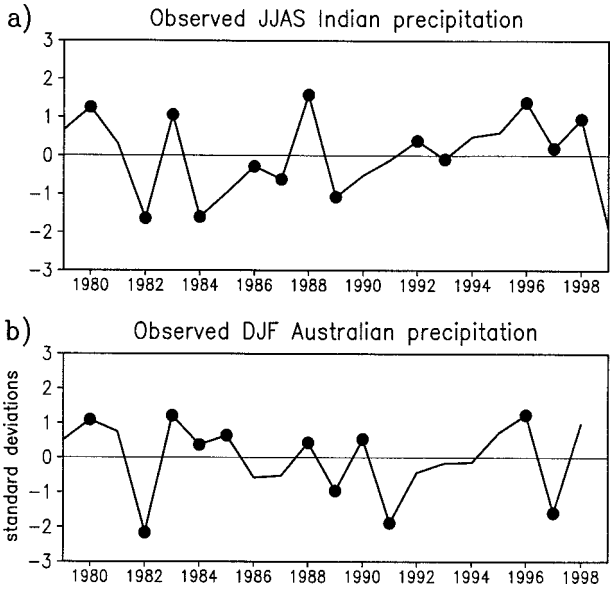

FIG. 1. (a) Time series of area-averaged Indian monsoon rainfall, JJAS, 1979–99, 5°–40°N, 60°–100°E; solid dots indicate TBO years when monsoon rainfall was relatively greater or less than preceding and following years. (b) Time series of area-averaged Australian monsoon rainfall, DJF, 1979–99, 20°S–5°N, 100°–50°E; solid dots as in (a).

is seen for the monthly data demonstrating that the TBO peak in the seasonal data in Fig. 2a is real and not an artifact of aliasing. Comparable spectra for Australian monsoon rainfall time series in Fig. 1b show TBO and ENSO peaks around 2.5 and 6 yr, respectively (Fig. 2c). Use of the monthly anomaly rainfall data to compute the spectra (Fig. 2d) also shows comparable significant TBO and ENSO peaks. Therefore, like the Indian monsoon, the TBO peak in Australian seasonal average monsoon rainfall is not due to aliasing.

Details for the hypotheses posed above are shown in the conceptual evolution for the TBO in Fig. 3. This is an updated portion of the schematic shown in Meehl (1997). For this hypothesized evolution, in the DJF season prior to a strong Indian monsoon there is a relatively weak Australian monsoon (Fig. 3a), with warm SST anomalies to the west in the Indian Ocean, to the east in the central and eastern Pacific, relatively cool SSTs north of Australia, and anomalously weak eastern and western Walker cells (EWC and WWC, respectively). As noted by Meehl (1997) for the case study of the 1987 and 1988 Indian monsoons, relatively strong convection over the western Indian Ocean and eastern African areas, along with strong convection over the central equatorial Pacific, are associated with an atmospheric Rossby wave response over Asia such that there is an anomalous ridge of positive 500-hPa heights and warm land temperatures. At the surface there are anomalous easterly winds in the southeastern tropical Indian and far western Pacific indicative of the weak Australian monsoon flow. These anomalous easterly winds in the western Pacific would induce upwelling Kelvin waves in the ocean that would propagate eastward. These would begin to raise the thermocline in the central and eastern Pacific over the course of the next few months as indicated in Fig. 3b. Meanwhile, in the far western Indian Ocean, there are westerly anomaly surface winds forming just south of the equator converging with the anomalous easterlies across most of the tropical Indian Ocean. This contributes to the anomalous convection over the western Indian Ocean and eastern Africa. The westerly wind anomalies near the equator would set off downwelling equatorial Kelvin waves in the ocean and deepen the thermocline in the eastern equatorial Indian Ocean in MAM (Fig. 3b).

In the MAM season prior to a strong Indian monsoon (Fig. 3b), the convective heating anomalies associated with the precipitation and SST anomalies would continue to contribute to the anomalous ridge over Asia and the warm land temperatures there. The upwelling Kelvin waves from the easterly anomaly winds in the western Pacific during DJF continuing into MAM would be acting to raise the thermocline in the central and eastern Pacific thus providing the conditions for a change in sign or transition of SST anomalies there from MAM to JJAS. In the Indian Ocean, westerly anomaly winds along the equator associated with stronger convection in the western Indian Ocean would act to raise the thermocline in the west and lower it in the east.

During JJAS (Fig. 3c), convection and precipitation over the Indian monsoon region is strong with strong WWC and EWC (note in this definition of the monsoon as in Fig. 1, land and ocean precipitation are included, the sum of which are presumed to be dynamically important for the TBO). Winds over the equatorial Indian Ocean remain westerly, and the shallow thermocline in the west is evidenced by anomalously cool SSTs appearing in the western equatorial Indian Ocean, and the beginning of a dipole of SSTs across the equatorial Indian Ocean. In the east there is a deep thermocline and warm SST anomalies. Heavy rainfall over parts of the Asian land areas contribute to cooler land temperatures. There are strong trades, and a shallow thermocline and cool SSTs in the central and eastern equatorial Pacific, thus completing the SST transition there, with a deep thermocline and warm SSTs in the western equatorial Pacific.

The SON season after the strong Indian monsoon (Fig. 3d) is characterized by a strong convective maximum traversing with the seasonal cycle to the southeast, encountering warm SSTs set up by the dynamical ocean response to the westerly winds in the equatorial Indian Ocean in JJAS. This dipole of SST anomalies in the Indian Ocean, historically a part of the TBO evolution, (Meehl 1987), is a consequence of the strong WWC and monsoon and wind interactions in the Indian Ocean, and may be associated with an extreme La Niña event in the Pacific. However, the tropical Pacific need not be in a La Niña extreme at this point in the TBO sequence,

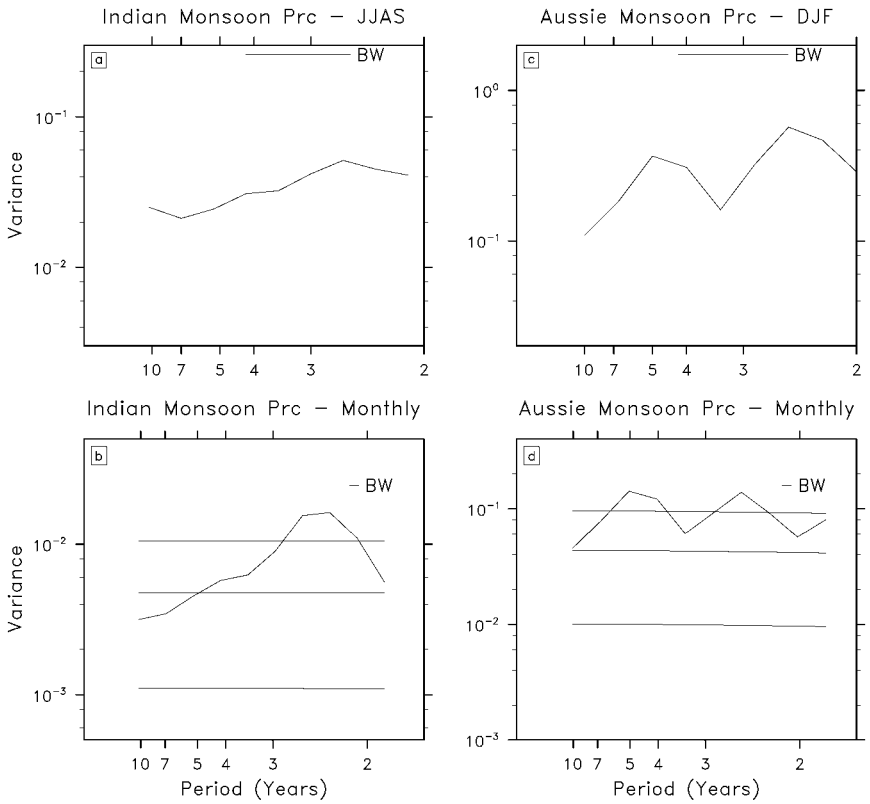

FIG. 2. (a) Spectra of seasonal Indian monsoon rainfall for time series in Fig. 1a, bandwidth is as indicated; (b) spectra of area-averaged monthly anomaly Indian monsoon region rainfall (all months), red noise estimate is middle line, bottom and top lines are 5% and 95% confidence limits, respectively, bandwidth is as indicated; (c) spectra of seasonal Australian monsoon rainfall for time series in Fig. 1b, bandwidth is as indicated; (d) spectra of area-averaged monthly anomaly Australian monsoon region rainfall (all months), red noise estimate is middle line, bottom and top lines are 5% and 95% confidence limits, respectively; bandwidth is as indicated.

but it is likely to have at least low-amplitude SST anomalies as shown in Fig. 3 due to the strong EWC and the coupled wind–ocean dynamical responses from the previous seasons.

Finally, in Fig. 3e in the DJF following a strong Indian monsoon, the strong convective maximum becomes established over the Australian monsoon region, with westerly anomaly winds dropping south of the equator in the southeastern tropical Indian Ocean as part of the anomalously strong WWC and surface inflow to the Australian monsoon. SSTs in the Indian Ocean have now completed the transition from mostly warm SST anomalies the previous DJF to mostly cool in Fig. 3e. Strong easterlies in the equatorial Pacific as part of the strengthened EWC are still associated with cool SSTs there. But anomalous westerlies in the far western equatorial Pacific associated with strong convection start to set off downwelling equatorial oceanic Kelvin waves that begin to deepen the thermocline to the east and set up the next transition to warm SSTs in the central and eastern equatorial Pacific the following MAM–JJAS. The combination of convective heating anomalies (weak over the western Indian–eastern Africa region and central Pacific, strong over the Australian monsoon), contribute to an anomalous Rossby wave response over Asia with a trough of negative 500-hPa height anomalies, and cold land temperatures. The sequence would follow, with opposite signs, to the following MAM, culminating in a weak Indian monsoon the following JJAS in this idealized sequence.

In section 2 we review the data, and in section 3 we quantify the strength of the associations within the seasons shown in Fig. 3. Then in section 4 we quantify the linkages in the MAM season to the following season (JJAS) Indian monsoon rainfall, and in section 5 we quantify similar associations for the SON conditions with DJF Australian monsoon rainfall. To identify the time evolution of the features associated with the transition conditions in MAM, in section 6 we calculate regressions from the singular value decomposition (SVD) expansion coefficient time series corresponding to the seasonal evolution depicted in Fig. 3. A summary of the results follows in Section 7.

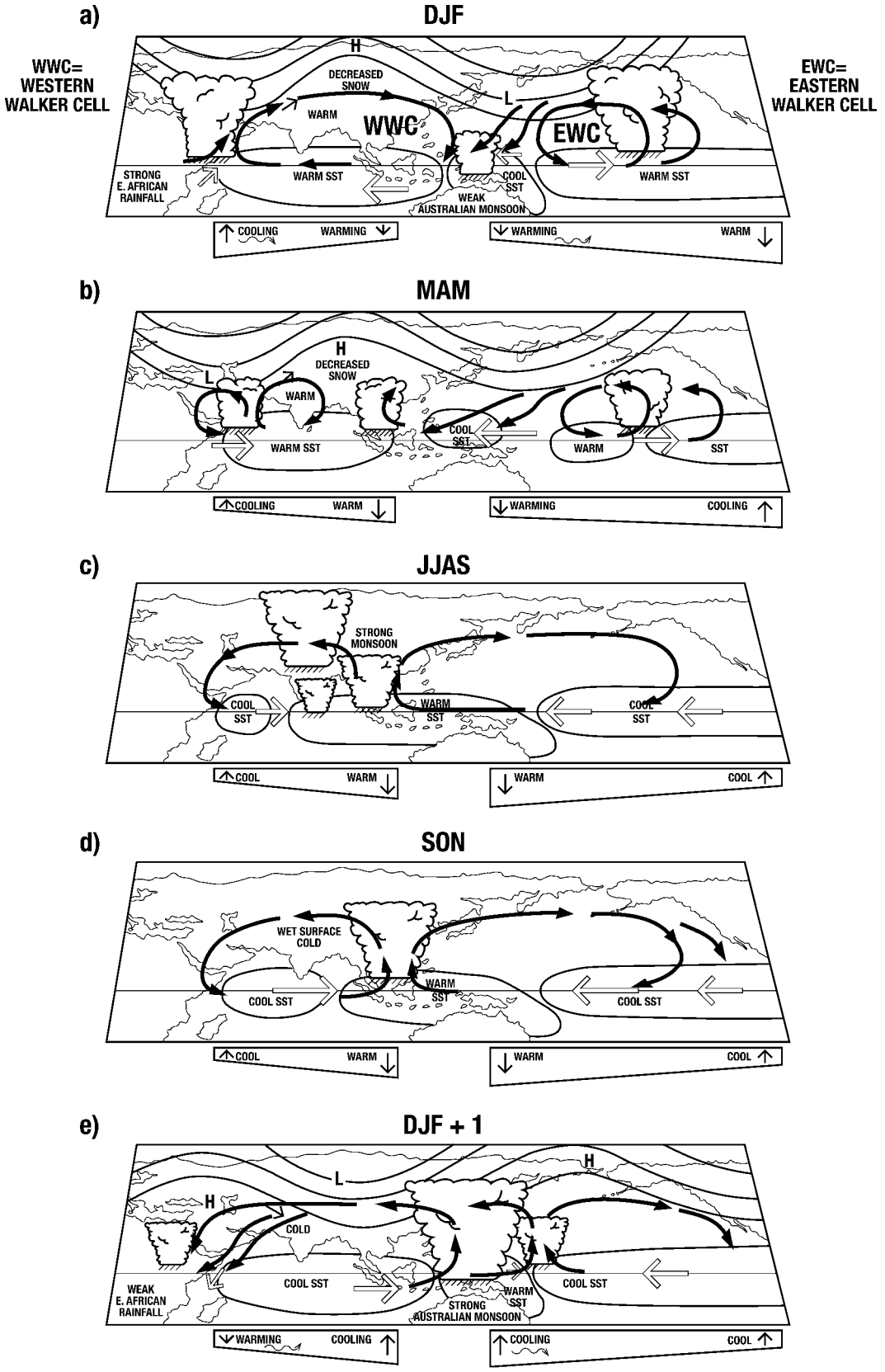
a)
DJF
WWC=
WESTERN
WALKER CELL
EWC=
EASTERN
WALKER CELL
H
L
DECREASED
SNOW
WARM
WWC
EWC
STRONG
E. AFRICAN
RAINFALL
WARM SST
COOL
SST
WARM SST
WEAK
AUSTRALIAN MONSOON
COOLING
WARMING
WARMING
WARM
b)
MAM
H
L
DECREASED
SNOW
WARM
COOL
SST
WARM SST
WARM
SST
COOLING
WARM
WARMING
COOLING
c)
JJAS
STRONG
MONSOON
COOL
SST
WARM
SST
COOL
SST
COOL
WARM
WARM
COOL
d)
SON
WET SURFACE
COLD
WARM
SST
COOL SST
COOL SST
COOL
WARM
WARM
COOL
e)
DJF + 1
L
H
H
COLD
WEAK
E. AFRICAN
RAINFALL
COOL SST
WARM
SST
COOL SST
STRONG
AUSTRALIAN MONSOON
WARMING
COOLING
COOLING
COOL

2. Data

We use 21 yr of observed data for the period January 1979–October 1999 when the gridded Climate Prediction Center (CPC) Merged Analysis of Precipitation (CMAP) precipitation data (Xie and Arkin 1996) are available, and 500-hPa heights and surface winds and temperatures from the National Centers for Environmental Prediction–National Center for Atmospheric Research (NCEP/NCAR) reanalysis data (Kalnay et al. 1996; Trenberth et al. 2001) for those same years. Therefore, there are 21 Indian monsoon years (1979–99), and 20 Australian monsoon years (1979–98), where December determines the year of the Australian monsoon from December–February (DJF; e.g., the Australian monsoon of 1980 would consist of December 1980, January 1981 and February 1981). All data are on a T42 grid.

3. DJF and MAM contemporaneous associations for Asian land temperatures

We first perform an SVD analysis to define the contemporaneous spatial associations between the transition conditions in DJF and MAM for Asian land temperatures. First looking at the DJF season (refer to Fig. 3a), we examine the relationship between precipitation anomalies in the tropical Indian and western Pacific region (20°S–20°N, 20°E–180°) and 500-hPa heights over Asia (30°–70°N, 50°–110°E). It was postulated earlier that convective heating anomalies in the Tropics could be associated with anomalous midlatitude circulation over Asia and, consequently, with surface temperature anomalies to contribute to anomalous meridional temperature gradients and subsequent monsoon strength. The patterns of the first SVD component are shown in Figs. 4a and b. As could be expected from the earlier case study and specified convective heating anomaly experiments (Meehl 1997), anomalous positive 500-hPa heights over Asia (Fig. 4a) are associated mainly with positive anomalies (greater than 0.5 mm day^{-1} corresponding to a unit standard deviation of the expansion coefficient of the first 500-hPa vector) over the equatorial Pacific east of Papua New Guinea extending east toward the date line and southwest over northern Australia (Fig. 4b). Additionally, there are negative precipitation regression anomalies north of Australia, near Borneo, and across the tropical Indian Ocean with values of greater than -0.5 mm day^{-1}. This pattern is consistent in some ways with the idealized configuration in Fig. 3a. However, the negative precipitation anomalies extend farther west as do the positive anomalies in the Pacific. Convective heating anomalies in the idealized convective heating anomaly experiment in Meehl (1997) with a comparable configuration to those in Fig. 4b contribute to a Rossby wave response over Asia in

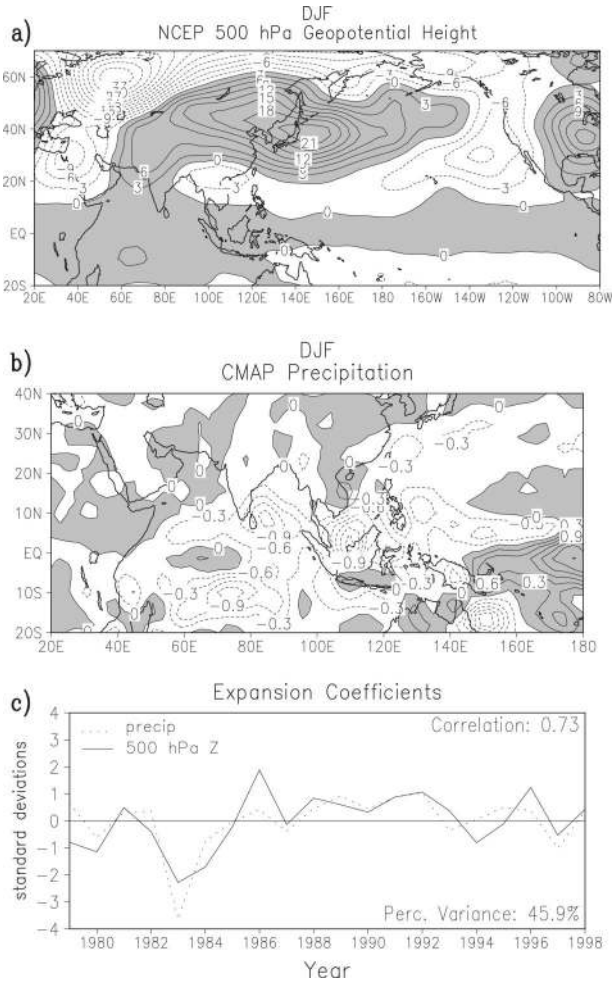

FIG. 4. The contemporaneous first SVD regression patterns relating (a) 500-hPa height over the area 30°–70°N, 50°–110°E during DJF [m (unit std dev of the expansion coefficient of the first DJF precipitation vector)$^{-1}$] to (b) DJF precipitation over the tropical region 20°N–20°S, 20°–180°E [mm day^{-1} (unit std dev of the expansion coefficient of the first 500-hPa height vector)$^{-1}$]. Note that the plots of the 500-hPa height and precipitation regressions here extend beyond their respective areas used in the SVD calculation.

←

FIG. 3. Schematic diagram indicating anomalous convective activity, SST anomalies, midlatitude circulation anomalies, surface wind anomalies, and equatorial Indian and Pacific Ocean thermocline orientation for hypothesized TBO evolution for (a) the Australian monsoon season prior to a strong Indian monsoon, (b) the MAM season before a strong Indian monsoon, (c) strong Indian monsoon season, JJAS, (d) SON season after a strong Indian monsoon and prior to a strong Australian monsoon, and (e) strong Australian monsoon following a strong Indian monsoon. Large arrows indicate surface wind anomalies, wedge-shaped outlines below each panel represent thermocline orientation, with the small arrows in those areas indicative of anomalous movement of the thermocline, and wavy arrows indicating Kelvin waves with the arrow at the end representing upwelling Kelvin waves (arrow pointing up), or downwelling Kelvin waves (arrow pointing down). Thick black arrows indicate EWC and WWC, respectively.

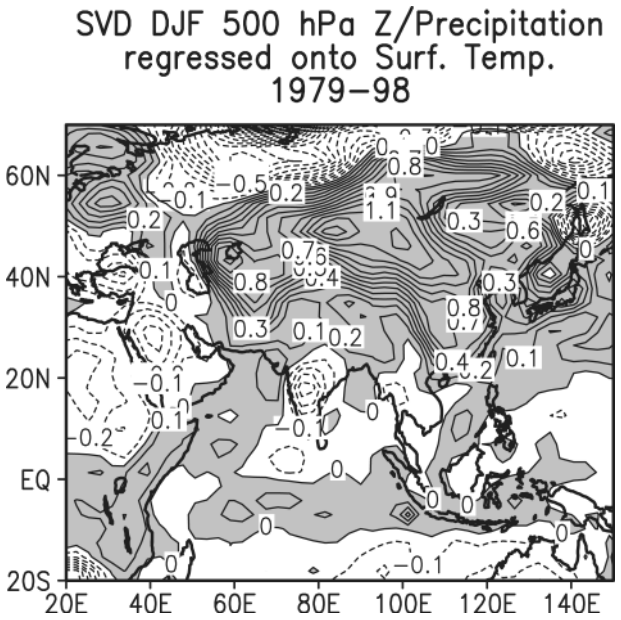

FIG. 5. Regression of the expansion coefficient of the first DJF 500-hPa vector from Fig. 4a with DJF surface temperature [°C (unit std dev of the expansion coefficient of the first 500-hPa vector)$^{-1}$].

the form of an anomalous ridge (positive 500-hPa anomalies in Fig. 3a; see also Meehl 1997, his Fig. 7). The expansion coefficient time series for the first SVD components are correlated at the +0.73 level (Fig. 4c) and explain 45.9% of the total squared covariance.

To calculate the association with Asian land temperatures, the expansion coefficient time series for 500-hPa height in Fig. 4c is regressed against surface temperatures over Asia and shown in Fig. 5. Again consistent with the idealized picture in Fig. 3a as well as the case study and the idealized convective heating anomaly experiment in Meehl (1997), positive regression values ranging from 0.2° to over 1.2°C per unit standard deviation of the expansion coefficient of the first 500-hPa vector are evident over much of Asia indicating that the anomalous 500-mb ridge in Fig. 4a is associated with anomalously warm land temperatures over Asia (Fig. 5), which contribute to an enhanced anomalous land–sea or meridional temperature gradient.

We next perform a similar SVD calculation for the MAM season (refer to Fig. 3b). In this case positive precipitation regression values of over 0.3 mm day^{-1} are evident over eastern Africa and the western Indian Ocean, and with values greater than +1.0 mm day^{-1} over the tropical Pacific near the date line (Fig. 6b), with negative values of roughly −1.0 mm day^{-1} north of Papua New Guinea. These precipitation anomalies and the implied convective heating anomalies are associated with positive 500-hPa height regression values ranging from +3 to over +12 m over Asia (Fig. 6a). The expansion coefficient time series for the first SVD components are correlated at the +0.79 level, and explain 37.5% of the total squared covariance.

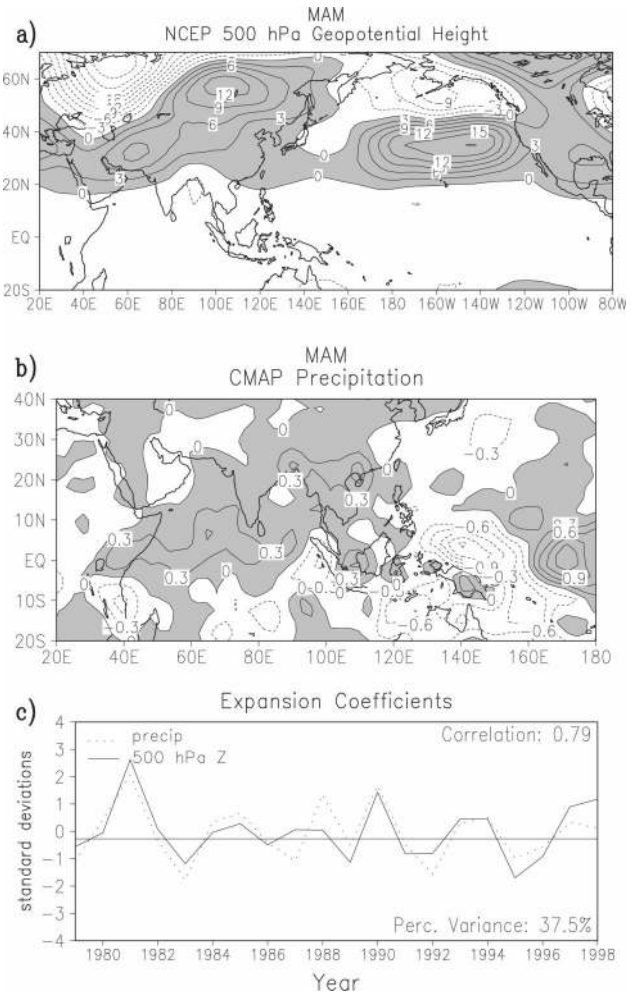

FIG. 6. The contemporaneous first SVD regression patterns relating (a) 500-hPa height over the area 30°–70°N, 50°–110°E during MAM [m (unit std dev of the expansion coefficient of the first MAM precipitation vector)$^{-1}$] to (b) MAM precipitation over the tropical region 20°N–20°S, 20°–180°E [mm day^{-1} (unit std dev of the expansion coefficient of the first 500-hPa height vector)$^{-1}$]. Note that the plots of the 500-hPa height and tropical precipitation regressions here extend beyond their respective areas used in the SVD calculation.

To make the linkage to Asian land temperatures, we regress the 500-hPa SVD expansion coefficient time series in Fig. 6c with Asian land temperatures and the result is shown in Fig. 7a. Some similar features to those in the DJF season in Fig. 5 are seen in Fig. 7a with positive regression values from about +0.2° to over +0.8°C per unit standard deviation of the expansion coefficient of the first 500-hPa vector indicating warmer land temperatures associated with the anomalous ridge in central Asia. The greatest positive regression values lie over northern Asia north of about 25°N indicating an enhanced meridional temperature gradient set up over Asian land areas. This seems counterintuitive since the traditional concept of ''land–sea temperature contrast'' would suggest that the greatest temperature gradient enhancement would set up between south Asia and the

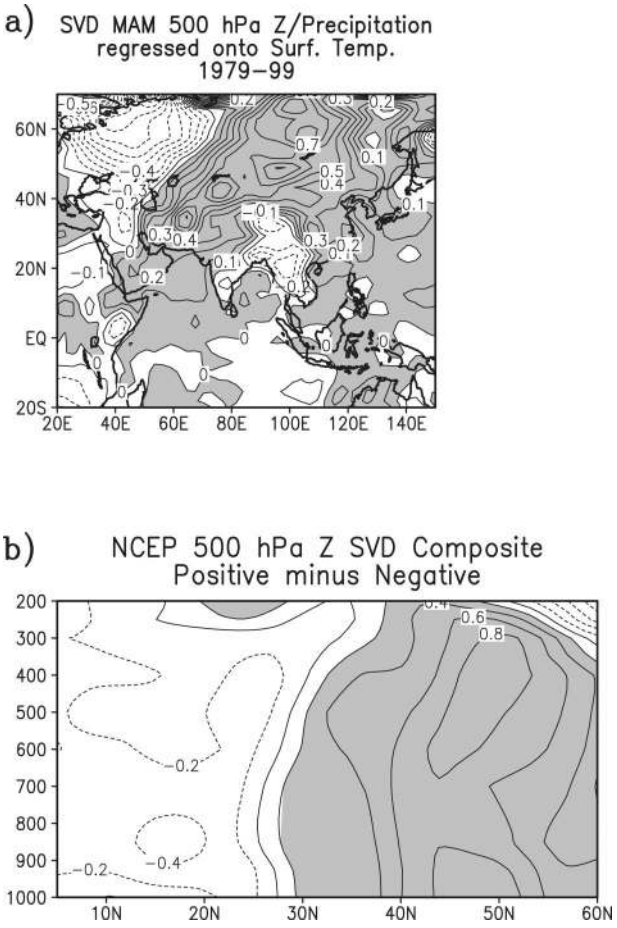

FIG. 7. (a) Regression of the expansion coefficient of the first MAM 500-hPa vector from Fig. 6a with MAM surface temperature [°C (unit std dev of the expansion coefficient of the first 500-hPa vector)$^{-1}$]; (b) vertical cross section, positive minus negative temperature composite years from the 500-hPa SVD expansion in (a), averaged from 70° to 90°E.

Indian Ocean. However, observational studies (Li and Yanai 1996; Bamzai and Shukla 1999) have shown that enhanced meridional temperature gradients over continental Asia can be associated with greater Indian monsoon rainfall, and that appears to be the case here. Additionally, the implication is that snow depth anomalies are symptomatic of large-scale atmospheric circulation changes (e.g., Bamzai and Shukla 1999; Kripalani and Kulkarni 1999), and not, by themselves, forcing agents for monsoon strength (Meehl 1997). The important quantity is the anomalous Asian land temperatures that contribute to meridional temperature gradients that affect monsoon strength.

Consequently, the positive surface temperature regression values over Asia are reflected by a warming through the depth of the troposphere in the composite differences for positive minus negative years of the 500-hPa expansion coefficient time series in Fig. 7b. Maximum positive differences above +0.8°C occur north of 40°N, while negative differences to the south are around −0.4°C. Therefore, the enhancement of the meridional tropospheric temperature gradient is on the order of nearly 1.5°C between about 20° and 45°N. GCM sensitivity experiments (Meehl and Arblaster 2001a, hereafter MEAR1) show that enhanced meridional temperature gradients can directly affect monsoon rainfall in some areas of south Asia independent of influences from the tropical Pacific or Indian Oceans.

Thus for the regional mechanism of tropical SST anomalies and associated precipitation and convective heating anomalies depicted in Fig. 3 prior to a relatively strong monsoon in the TBO, the observations for the 1979–99 period seem to be consistent with the earlier case study and idealized convective heating anomaly experiment shown by Meehl (1997). The results thus far suggest that, as a result of air–sea coupling, the SST anomalies in the tropical Indian and Pacific Oceans are associated with precipitation and convective heating anomalies that are positive in the western equatorial Pacific, negative northwest of Australia and over the Indian Ocean, and are associated with an anomalous ridge of positive 500-hPa heights over Asia and warm land temperatures over central Asia. These conditions would lend themselves to an enhanced meridional temperature gradient and a strong subsequent Indian monsoon in JJAS (Fig. 3c). We will analyze the role of surface wind forcing associated with the air–sea coupling in sections 6 and 7.

4. TBO transition conditions from MAM to JJAS

We next perform lagged SVD analyses to define the maximum covariability of spatial associations between the transition conditions in the March–May (MAM) season with rainfall over the Indian region (5°–40°N, 60°–100°E) for the monsoon season of June–September (JJAS). A multivariate regression analysis technique could also serve to extract forcing and response, but the SVD analysis provides expansion coefficient time series that can be used to calculate the strength of year-to-year associations of the various transition conditions. For MAM, we use 1) 500-hPa height anomalies over Asia which, when positive, represent atmospheric circulation anomalies (e.g., warm air advection from the south) and associated anomalously warm Asian land temperatures with an enhanced meridional temperature gradient that could strengthen subsequent monsoon rainfall as suggested in Figs. 6 and 7 (Li and Yanai 1996); 2) Indian Ocean SSTs that, if anomalously warm, could provide a moisture source for greater monsoon rainfall through enhanced evaporation (Rao and Goswami 1988; Trenberth 1999; Clark et al. 2000); and 3) eastern equatorial Pacific SSTs that could affect monsoon rainfall through changes in the EWC (the large-scale atmospheric east–west circulation; Rasmusson and Carpenter 1983).

For positive 500-hPa height anomalies over south Asia in MAM (on the order of 5 m per unit standard deviation of the expansion coefficient of the first pre-

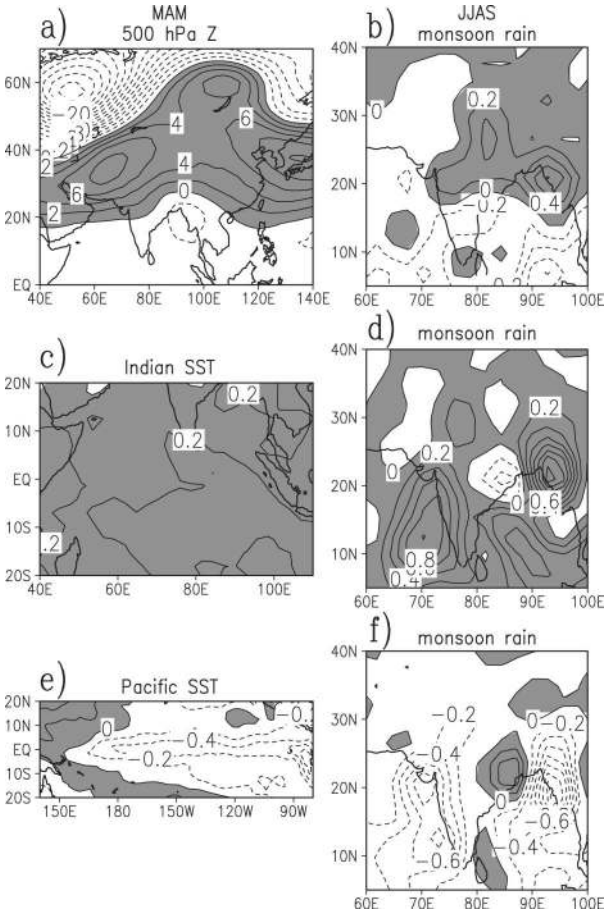

FIG. 8. The first component SVD regression patterns, 1979–99, relating (a) 500-hPa height over the area 30°–70°N, 50°–110°E during MAM [unit std dev of the expansion coefficient of the first JJAS precipitation vector)$^{-1}$] to (b) JJAS precipitation over the Indian region 5°–40°N, 60°–100°E [mm day^{-1} (unit std dev of the expansion coefficient of the first 500-hPa height vector)$^{-1}$; note that the plot of the 500-hPa height regressions extends beyond the area used in the SVD calculation]; (c) MAM surface temperature for the area in the tropical Indian Ocean 20°S–20°N, 40°–110°E [°C (unit std dev of the expansion coefficient of the first JJAS precipitation vector)$^{-1}$], to (d) JJAS precipitation over the Indian region 5°–40°N, 60°–100°E [mm day^{-1} (unit std dev of the expansion coefficient of the first surface temperature vector)$^{-1}$]; (e) MAM surface temperature for an area in the eastern equatorial Pacific 20°S–20°N, 150°E–80°W [°C (unit std dev of the expansion coefficient of the first JJAS precipitation vector)$^{-1}$], to (f) JJAS precipitation over the Indian region 5°–40°N, 60°–100°E [mm day^{-1} (unit std dev of the expansion coefficient of the first Pacific surface temperature vector)$^{-1}$]. Shaded areas denote positive values.

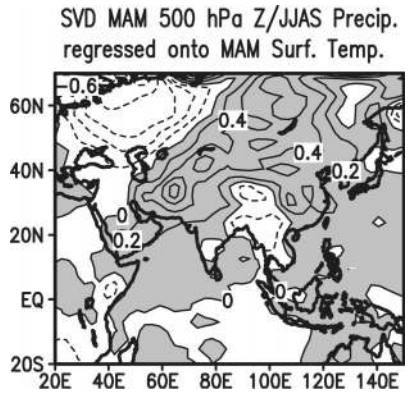

FIG. 9. Regression of the expansion coefficient of the first MAM 500-hPa vector from Fig. 8a with MAM surface temperature [°C (unit std dev of the expansion coefficient of the first MAM 500-hPa vector)$^{-1}$].

cipitation vector, Fig. 8a), there are positive JJAS monsoon precipitation anomalies over much of northern and northeastern India, Bangladesh, and Burma (on the order of about 0.3–0.4 mm day^{-1} per unit standard deviation of the expansion coefficient of the first 500-hPa vector, Fig. 8b). The expansion coefficient time series for the first SVD components (not shown) are correlated at the +0.76 level, and explain 39.3% of the total squared covariance. Regressing the lagged SVD expansion coefficient time series from Fig. 8a onto the surface temperature shows positive MAM regression values of greater than 0.5°C per unit standard deviation of the expansion coefficient of the first 500-hPa vector over much of southwest and central Asia (Fig. 9) similar to the simultaneous SVD relationship in Fig. 7a.

For positive SSTs in the Indian Ocean in MAM (Fig. 8c), there are positive JJAS precipitation anomalies over southwestern and southern India, Burma, and the Arabian Sea and Bay of Bengal (Fig. 8d). The expansion coefficient time series for the first SVD components are correlated at the +0.75 level, and and explain 58.0% of the total squared covariance. Negative SST anomalies in the equatorial eastern Pacific in MAM (Fig. 8e) are associated with positive JJAS monsoon precipitation anomalies over Sri Lanka and areas of eastern India (Fig. 8f). The expansion coefficient time series for the first SVD components are correlated at the +0.70 level, and explain 39.2% of the total squared covariance. However, as shown in Fig. 3 and discussed later, the SSTs in the eastern Pacific transition from MAM to JJAS. Therefore, the negative SST anomalies in Fig. 8e are actually associated with positive SST anomalies during the JJAS season, which would contribute to suppressing the JJAS monsoon rainfall over most of the domain as seen in Fig. 8f. When we varied the boundaries of the regions used in the SVD calculation, the patterns were not significantly affected.

We use the first SVD components for three separate conditions since those are the dominant relationships accounting for a majority of the squared covariance (the second SVD components for the three transition conditions discussed in Figs. 8a,b; 8c,d; and 8e,f account for 17.9%, 14.2%, and 18.5%, respectively, with the third through fifth components for all three accounting for considerably less). However, there clearly is no requirement that the first SVD components from the three transition conditions be orthogonal. In fact, comparing Fig. 8d and 8f, there are indications that the patterns of

precipitation for these two transition conditions are related. Positive MAM SSTs in the Indian Ocean also can occur with positive SSTs in the Pacific in MAM (which would transition to negative anomalies in JJAS as noted above and discussed later). Thus the two ocean basins are linked in some years in their relation to the patterns of JJAS Indian monsoon rainfall. (We will address this further in Figs. 14 and 15.)

Previous studies (e.g., Kawamura 1998; Yasunari and Seki 1992; Lau and Yang 1996; Clarke et al. 1998) have shown various connections between Indian monsoon rainfall, anomalous atmospheric circulation over Asia in the seasons prior to the monsoon, and tropical Indian and Pacific SST anomalies. The advantage of the present SVD technique is that we can quantify the individual associations year by year to clarify which years the various associations are working independently and which years they are linked. To that end we then calculate spatial anomaly pattern correlations between the observed JJAS rainfall patterns and the SVD projections individually and cumulatively (Lau and Wu 1999; MEAR2). The cumulative contribution up to the *k*th SVD for *i* transition conditions (using the first SVD component from each of the three transition conditions, so $i = 3$ here) to the actual observed rainfall anomaly for the *j*th year is given by

$$A_{i,j} = \left\langle O_j, \sum_{k=1}^{i} S(k)C(k)_j \right\rangle,$$

where $\langle\ \rangle$ is the spatial anomaly pattern correlation over the Indian monsoon region. *S* is a normalized precipitation SVD pattern for JJAS associated with a MAM transition condition (Fig. 8), *C* is the precipitation SVD expansion coefficient for that year, and *O* is the observed JJAS Indian monsoon rainfall anomaly. Each anomaly pattern correlation is first calculated separately (Fig. 10a), and then the cumulative value is computed (Fig. 10b). A large positive correlation indicates a strong association with the observed monsoon rainfall pattern for that year.

The association between tropical Pacific and Indian SSTs and the pattern of Indian monsoon rainfall is large in some El Niño (e.g., 1982) and La Niña (e.g., 1988) years when both have pattern correlation values greater than nearly +0.4 in Fig. 10a. In other years they act independently (e.g., 1992 and 1994). This demonstrates that in some years the Indian Ocean can provide a regional input to monsoon rainfall separate from large-scale influences emanating from the Pacific. Interestingly, the Indian and Pacific conditions follow each other fairly closely before about 1990, but less so after that. This likely relates to the sustained warm conditions in the Pacific in the early 1990s and the consequent effects in the Indian Ocean (Allan and D'Arrigo 1999).

In several years the regional 500-hPa atmospheric circulation–Asian land–meridional temperature gradient condition is more dominant (e.g., 1980, 1990, 1993, 1995, and 1996) with values above +0.4 in Fig. 10a. Connections between tropical Pacific SSTs, 500-hPa height, and Indian SST are strong in 1984, 1985, and 1989 when all have values near to or greater than +0.4, thus confirming some of studies cited earlier. In other years (1991, 1995, 1998) the three conditions are unrelated with widely different values. In 1984 when all

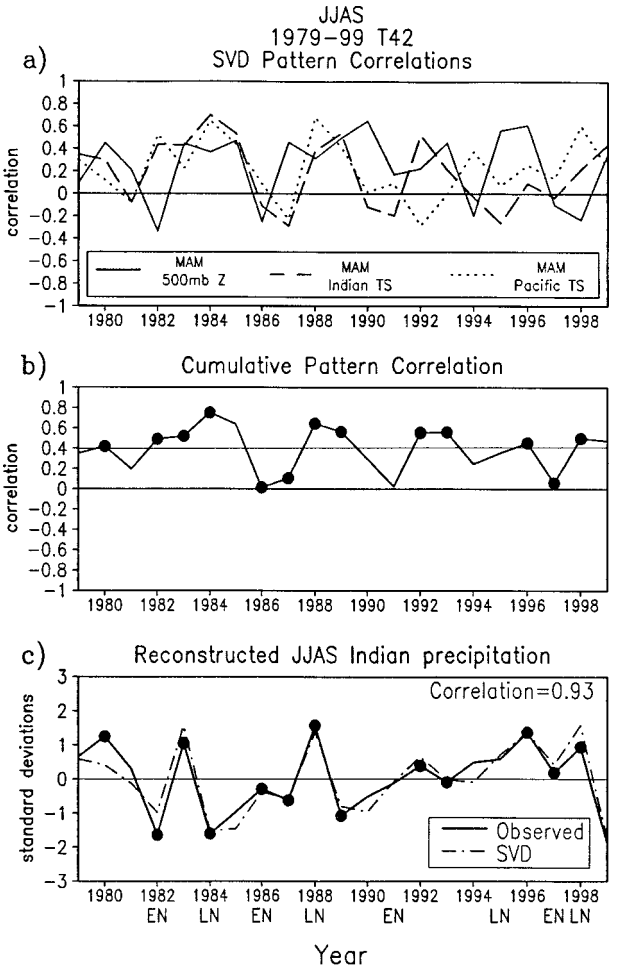

FIG. 10. (a) Time series, 1979–99, of individual anomaly pattern correlations for the regional (500-hPa height, Indian Ocean SST) and large-scale (Pacific surface temperatures) MAM SVD-derived conditions from Fig. 8 with observed JJAS Indian monsoon rainfall patterns for the area 5°–40°N, 60°–100°E, (b) cumulative anomaly pattern correlations for Indian monsoon rainfall combining the three conditions in (a); nominal significance level of 0.40 (marked in Fig. with thin solid line) is determined by a Monte Carlo technique described in the text; (c) time series of an index of Indian monsoon strength (area-averaged over Indian region, all points, 5°–40°N, 60°–100°E) of the cumulative precipitation patterns in (b) derived from the SVD analysis normalized by their respective standard deviations (dash–dot line), and the full area-averaged normalized precipitation index over the same region calculated from the original precipitation data (solid line as in Fig. 1a). El Niño (EN) and La Niña (LN) onset years defined in text are denoted beneath the corresponding years. Solid dots in (b) and (c) indicate relatively strong and weak monsoon years in relation to previous and following years for the observed index in (c).

three transition conditions have high values (Fig. 10a), the cumulative value is about +0.8 (Fig. 10b) indicating over 60% of the spatial variance of the pattern of monsoon precipitation is accounted for in that year. However in 1986 when all of the three conditions are near zero for their individual associations, the cumulative pattern correlation is also near zero indicating other processes or internal dynamics are more important for the pattern of monsoon rainfall in that year. The point is that in any given year, we quantify the magnitude of the associations of the various transition conditions (either none, some, or all) in MAM with the subsequent JJAS monsoon rainfall.

A nominal significance level of 0.4 in Fig. 10b is determined by a Monte Carlo technique whereby the seasonal pattern correlations from the SVD components are scrambled to randomly generate 865 sample pattern correlations with no overlap with the actual cumulative pattern correlations in Fig. 10b. A Student's *t*-test is performed to determine that the mean value of 0.4 is significantly different from the mean of the random samples (using 884 degrees of freedom) at greater than the 1% level. For the 21 yr considered here from 1979 to 1999, 12 (57%) exceed this nominal significance level.

To relate the precipitation anomaly patterns to an area-averaged monsoon index and consequently the magnitude of the TBO, regressions of the SVD expansion coefficient time series and the SVD rainfall patterns over the Indian region are used to produce a cumulative area-averaged Indian rainfall index (Fig. 10c). The correlation between the SVD-derived normalized cumulative index of monsoon ''strength'' and the full area-averaged normalized index from the original CMAP precipitation data is +0.93 (significant at greater than the 1% level) thus showing the SVD-derived index can capture 86% of the variance of the full index. Therefore, in Fig. 10 we quantify *individual contributions to the pattern of monsoon rainfall* from several transition conditions (Fig. 10a), the *cumulative contributions to the pattern of monsoon rainfall* (Fig. 10b), and a reconstructed area-averaged index of *strength of the monsoon* (Fig. 10c).

As noted earlier in relation to Fig. 1, TBO monsoon years can be defined as a monsoon index value greater than the previous or following year, or less than the previous or following year (Meehl 1987). These are denoted in Fig. 10c (as in Fig. 1a) for 13 yr (out of 21 yr total). We define onset years for El Niño (1982, 1986, 1991, 1997) and La Niña (1984, 1988, 1995, 1998) as the initiation of a 5-month running mean area-averaged SST anomaly in the eastern tropical Pacific Niño-3 area (5°N–5°S, 150°–90°W) of at least ±0.5°C for two consecutive seasons after the MAM transition season over the following 1-yr period. Of the TBO years, 1982, 1986, 1997 are El Niño onset years, and 1984, 1988, and 1998 are La Niña onset years for a total of 6 TBO years out of 8 possible ENSO onset years. That leaves 1980, 1983, 1987, 1989, 1992, 1993, and 1996 as 7 non-ENSO onset years that also are contributing to the interannual flip-flops that characterize the TBO in monsoon rainfall. In Fig. 10b, 10 of these 13 TBO years have greater than the nominal significance value of 0.4, indicating that the transition conditions in Fig. 8 are strongly associated with 77% of the years with TBO transitions.

Another way of quantifying the TBO is to first compute spectra of area-averaged time series of SVD-reconstructed JJAS monsoon rainfall as in Fig. 10c for each condition in Fig. 10a individually and then cumulatively, and then average the power in the TBO band of 2.1–2.8 yr. The TBO spectral density [$(\text{mm}^2\ \text{day}^{-2}\ \text{yr}) \times 10^{-1}$] for the individual 500-hPa SVD is 0.1. Adding the contribution of the Pacific SST conditions increases the TBO amplitude to 2.2. Including the effects from the Indian Ocean SST conditions, such that all three transition conditions are accounted for, increases TBO amplitude to 8.3, which is 8% greater than the spectral density in the ENSO periods of 3–7 yr derived in the same way. This increase in TBO amplitude with the inclusion of Indian Ocean SSTs is related to area-averaged precipitation and is not as clear for the pattern correlations in Fig. 10a. In that figure, neither of the three conditions exhibits a dominant overall effect on the pattern of monsoon rainfall. For the monsoon index computed from the original data (solid line in Fig. 10c, and spectra shown in Fig. 2c), spectral density in the TBO periods is 52% greater than in the ENSO periods. Thus there is more power in the TBO periods than the ENSO periods for both the reconstructed and original monsoon indices. These results confirm the hypothesis above such that the more transition conditions included in the analysis and the more these processes work, the more likely it is for a transition to occur in a given year, and thus the higher the amplitude of the TBO.

To determine to what extent ENSO years influence the SVD associations, in Fig. 11 we perform the SVD analyses in Fig. 8 again, but remove the ENSO onset years (defined earlier in Fig. 10). If the patterns with and without ENSO years are similar, we can conclude that similar sets of processes are occurring in ENSO and non-ENSO years, the latter encompassing the greater number of years of the TBO with a 2–3-yr period. Indeed the SVD patterns are very similar. The pattern correlation for MAM 500-hPa height in Figs. 8a and 11a is +0.96, and for corresponding JJAS monsoon rainfall in Figs. 8b and 11b is +0.86. The pattern correlation for MAM Pacific SST in Figs. 8e and 11e is +0.96, and for associated JJAS monsoon rainfall in Figs. 8f and 11f is +0.89. This indicates that for the 500-hPa Asian land meridional temperature gradient, and for the tropical Pacific SST conditions, comparable processes are taking place in ENSO and TBO, thus inextricably linking TBO and ENSO for those processes. The pattern correlations between Indian Ocean SSTs and associated monsoon rainfall patterns without ENSO (Figs. 11c,d) are somewhat lower than with all years

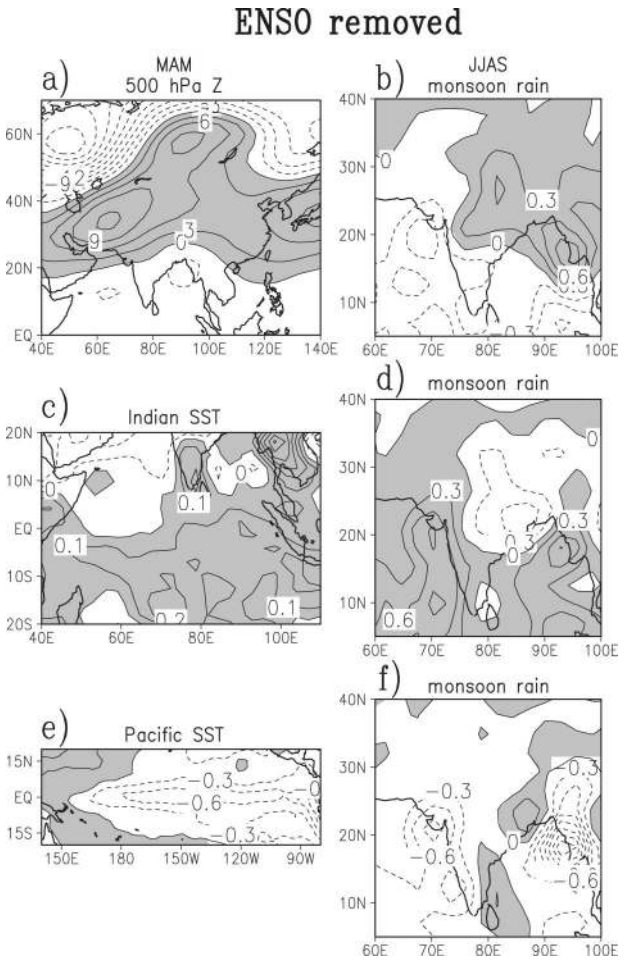

FIG. 11. Same as in Fig. 8 except for the El Niño and La Niña onset years (noted in Fig. 10c) are removed. Removal of 4 El Niño onset years and 4 La Niña onset years leaves 13 yr in this SVD analysis.

included (Figs. 8c,d). The pattern correlations for Indian SSTs in Figs. 8c and 11c are +0.71, and for the corresponding monsoon rainfall in Figs. 8d and 11d +0.53. In the non-ENSO years the warmer SSTs are concentrated mostly south of India (Fig. 11c) and are associated with increases in JJAS Indian monsoon rainfall over mostly ocean areas, with suppressed rainfall over central and northeastern India (Fig. 11d). Thus we conclude that the Indian Ocean does not act as strongly in unison with the tropical Pacific during MAM in non-ENSO years in their contribution to the TBO as has been suggested by recent studies for other parts of the year (Webster et al. 1999; Saji et al. 1999; Chang and Li 2000; Loschnigg and Webster 2000).

5. SON to DJF transitions

Following the progression in Fig. 3, we now turn to the subsequent Australian monsoon in DJF. Though we discussed earlier that we identified ''transition'' conditions for the Australian monsoon, it is well known that there is persistence from consecutive Indian to Australian monsoons, with a strong Australian monsoon often following a strong Indian monsoon and vice versa for weak Indian and Australian monsoons (e.g., Shukla and Paolino 1983; Kiladis and van Loon 1988; Webster and Yang 1992). This is represented by the strong Indian monsoon followed by a strong convective maximum in SON over Southeast Asia leading to a strong Australian monsoon the following DJF in the idealized depiction in Fig. 3.

To quantify this association for the full time series from 1979 to 1999, we perform SVD analyses similar to that in the Indian monsoon using conditions in SON that are hypothesized to lead to a strong Australian monsoon in Fig. 3d. These include SON precipitation from the area of maximum precipitation over Southeast Asia (10°N–10°S, 90°–130°E); Indian Ocean SST (equator to 25°S, 90°–120°E); and Pacific SST (20°N–20°S, 150°E–80°W) and their respective associations with Australian monsoon rainfall (5°N–20°S, 100°–150°E) in DJF.

Results in Fig. 12 from the SVD analyses show a ''dipole'' of SST in the Indian Ocean as depicted in Fig. 3c (warm in the eastern equatorial Indian and cool to the west). The positive SST regression values over the ocean areas of Southeast Asia and north of Australia are several tenths of a degree per unit standard deviation of the expansion coefficient of the first precipitation vector in Fig. 12a. This is associated with positive precipitation regression values of over +1.0 mm day^{-1} over parts of Indonesia, Papua New Guinea, and the southeast tropical Indian Ocean during the following DJF with a correlation of expansion coefficient time series of +0.72 accounting for 82.5% of the total squared covariance (Fig. 12b). Similarly, cold Pacific SSTs in SON with regression values of around −1.0°C in Fig. 12c are associated with a comparable pattern and magnitude of Australian monsoon rainfall anomalies with a correlation of expansion coefficient time series of +0.79 accounting for 94.5% of the total squared covariance (Figs. 12c,d). Thus, as for the Indian monsoon, the tropical Indian and Pacific Oceans are strongly connected in their patterns of SSTs and associated Australian monsoon rainfall.

The strong convective maximum over Southeast Asia during SON (positive regression values of around 0.2–0.3 mm day^{-1}) is associated with enhanced precipitation over most of the Australian monsoon domain again with a comparable pattern and magnitude to the other two conditions in Figs. 12b and 12d. The correlation of expansion coefficient time series is +0.79 accounting for 94.2% of the total squared covariance (Figs. 12e,f).

Judging from the similarity of the Australian monsoon patterns and the large percent covariance explained for the three SON conditions in Fig. 12, it would appear that the conditions prior to the Australian monsoon are less independent from each other than for the MAM conditions for the Indian monsoon in Fig. 8. Indeed

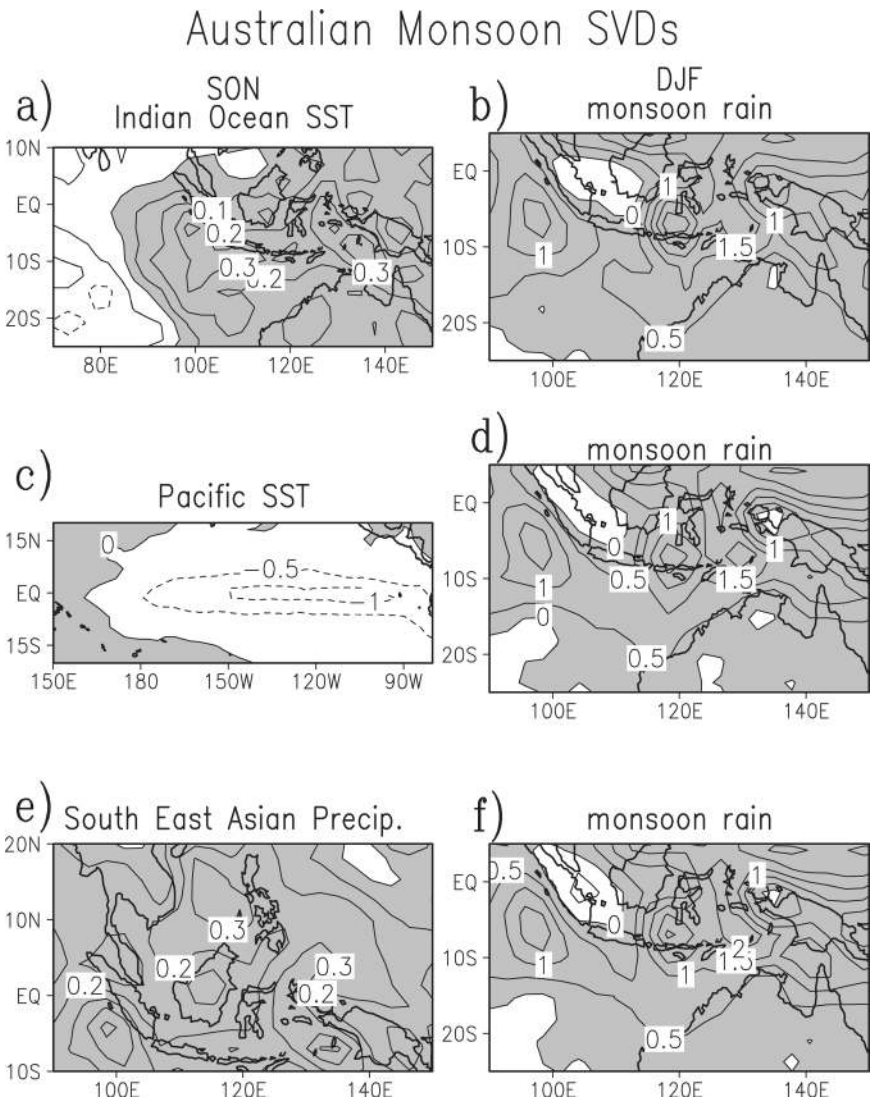

FIG. 12. The first component SVD regression patterns, 1979–99, relating (a) surface temperatures in the eastern Indian Ocean region from 25°S to the equator, 90°–120°E during SON [°C (unit std dev of the expansion coefficient of the first DJF precipitation vector)$^{-1}$] to (b) DJF precipitation over the Australian monsoon region 20°S–5°N, 100°–150°E [mm day^{-1} (unit standard deviation of the expansion coefficient of the first SON surface temperature vector)$^{-1}$], (c) SON surface temperature for the area in the tropical Pacific Ocean 20°S–20°N, 150°E–80°W [°C (unit std dev of the expansion coefficient of the first DJF precipitation vector)$^{-1}$], to (d) DJF precipitation over the Australian monsoon region 20°S–5°N, 100°–150°E [mm day^{-1} (unit std dev of the expansion coefficient of the first surface temperature vector)$^{-1}$], (e) SON precipitation over the Southeast Asian area 10°S–10°N, 90°–130°E [mm day^{-1} (unit std dev of the expansion coefficient of the first DJF precipitation vector)$^{-1}$], to (d) DJF precipitation over the Australian monsoon region 20°S–5°N, 100°–150°E [mm day^{-1} (unit std dev of the expansion coefficient of the first SON Southeast Asian precipitation vector)$^{-1}$]. Note that the regression plots can extend beyond their respective areas used in the SVD calculation. Shaded areas indicate positive values.

constructing the single SVD pattern correlations (Fig. 13a) and cumulative pattern correlations (Fig. 13b) shows that the three conditions in SON act in unison in most years, either all contributing to the pattern of subsequent monsoon rainfall or not. Clearly they act much more uniformly than the transition conditions for the Indian monsoon in Fig. 10. This is likely due to the seasonal coherence of the strength of the convective maximum as it evolves from the Indian to the Australian monsoon system mentioned earlier and that, once set in JJAS, has greater persistence as the seasonal cycle progresses from JJAS to the following DJF as depicted in Fig. 3. Since this coherence of the system also involves tropical Pacific and Indian Ocean SST anomalies as

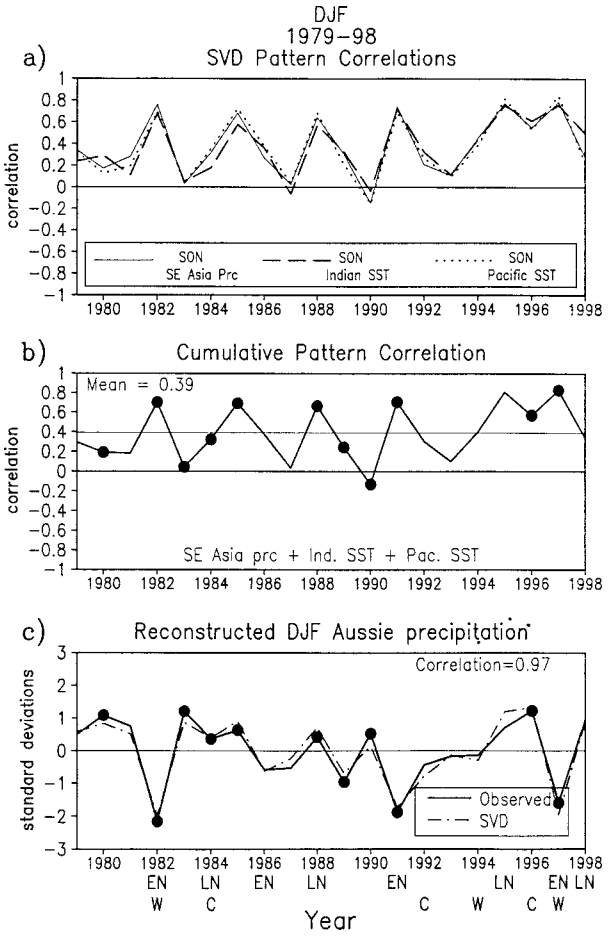

FIG. 13. (a) Time series, 1979–99, of individual anomaly pattern correlations for the regional (Indian Ocean SST and Southeast Asian precipitation) and large-scale (Pacific surface temperatures) SON SVD-derived conditions from Fig. 12 with observed DJF Australian monsoon rainfall patterns for the area 20°S–5°N, 100°–150°E, (b) cumulative anomaly pattern correlations for Australian monsoon rainfall combining the three conditions in (a); nominal significance level of 0.40 (marked in Fig. with thin solid line) is determined by a Monte Carlo technique described in the text; (c) time series of an index of Australian monsoon strength (area-averaged over Australian monsoon region, all points, 20°S–5°N, 100°–150°E) of the cumulative precipitation patterns in (b) derived from the SVD analysis normalized by their respective std dev (dash–dot line), and the full area-averaged normalized precipitation index over the same region calculated from the original precipitation data (solid line as in Fig. 1b). EN and LN onset years defined in text are denoted beneath the corresponding years. Solid dots in (b) and (c) indicate relatively strong and weak monsoon years in relation to previous and following years for the observed index in (c). Warm (W, western Indian Ocean warmer than east, ''positive dipole'') and cold (C, western Indian Ocean colder than east, ''negative dipole'') extreme SST dipole years from Saji et al. (1999) also noted below years at bottom.

shown in Figs. 12 and 13, these must be related to upper-ocean temperature anomalies and ocean dynamics. This is addressed in a subsequent paper (Meehl et al. 2002, manuscript submitted to *J. Climate*).

The reconstructed area-averaged rainfall index in Fig. 13c from the SVD patterns is highly correlated with the total area-averaged index from the original precipitation data (+0.97) indicating, as for the Indian monsoon rainfall data, that the SVD reconstructions can reproduce much of the original time series of monsoon strength (94% of the variance) using just the first SVD components. The tendency for persistence from Indian to Australian monsoon noted above can be demonstrated by correlating the JJAS Indian monsoon area-averaged precipitation index (Fig. 10c) with the following DJF Australian monsoon area-averaged precipitation index (Fig. 13c). This value is +0.55, which is significant at the 1% level corroborating earlier results that in many years a strong Indian monsoon is followed by a strong Australian monsoon, and vice versa for weak monsoons. Also it is clear from Fig. 3 why there is little persistence from Australian monsoon to subsequent Indian monsoon since the TBO transition period is across the seasons MAM–JJAS.

As noted above, the SST dipole in the Indian Ocean with maximum values in the SON season is seen here to be an integral part of the TBO and is a consequence of coupled air–sea interaction directly involving the Indian and Australian monsoons. Extreme dipole mode events from Saji et al. (1999) are 1982, 1994, and 1997 (warm or ''positive dipole'' with positive SST anomalies in the western Indian and negative in the east, opposite in sign to the depiction in Figs. 3 and 12), and 1984, 1992, and 1996 (cold or ''negative'' dipole with signs as depicted in Figs. 3 and 12). Thus the ''W'' in Fig. 13c refers to positive dipole (warm west and cool east), and the ''C'' to negative dipole (cool east and warm west). For those 6 strong dipole mode events, 5 are significantly accounted for by the Indian Ocean SST SVD pattern in Fig. 13a (dashed line) with values near or greater than +0.4 (all but 1984). All are also seen to act in unison with the tropical Pacific in Fig. 13a (comparable evolution of dashed and dotted lines), though only 1982 and 1997 are El Niño onset years, and 1984 is a La Niña onset year. Therefore, half (three) of the extreme Indian Ocean dipole years are non-ENSO onset years consistent with previous observations that extreme Indian Ocean dipole years can occur without an extreme ENSO year. This also has been noted to occur in a coupled GCM (Iizuka et al. 2000). However, Fig. 13a does indicate a linkage to the tropical Pacific, through coupled interactions involving the large-scale east–west circulation (WWC and EWC) involved with the Asian–Australian monsoon system and coupled ocean dynamics (Fig. 3). It is also worth noting that the Indian Ocean dipole pattern with significant pattern correlations (with subsequent Australian monsoon rainfall) above +0.4 in Fig. 13a occurs in other years as well (1985, 1986, 1988, 1991, 1995, and 1998).

For the reconstructed Australian monsoon precipitation index in Fig. 13c, all three extreme warm or positive dipole events are associated with below-normal Australian monsoon rainfall, and two out of three cold or negative dipole events occur in years with above-normal

Australian monsoon rainfall (all but 1992). This supports the connection between the Indian Ocean SST dipole pattern in SON with the strength of the DJF Australian monsoon and the TBO.

If TBO years are defined in a similar way to the Indian monsoon (denoted by the solid dots in Fig. 13c), 6 of the 11 TBO years are significantly accounted for by the cumulative pattern correlations in Fig. 13b (values near or above +0.4). It was noted earlier that there is seasonal persistence from Indian to Australian monsoon as indicated by an overall correlation between Indian and the subsequent Australian monsoon of +0.55. This is also seen in the TBO years. For the 13 TBO years defined for the Indian monsoon in Fig. 10c, only 12 are eligible for continuation to the Australian monsoon (even though 1998 is an above-normal Australian monsoon, we cannot define it as a TBO year relatively stronger than the preceding and following years since the precipitation data end in October 1999 and we do not have the 1999 Australian monsoon data). For those 12 TBO Indian monsoon years, 8 or 67% correspond to like sign TBO years in the Australian monsoon, 4 relatively strong (1980, 1983, 1988, 1996) and 4 relatively weak (1982, 1984, 1989, 1997). Of those 8, only 4 are ENSO onset years (1982 and 1997 El Niño, 1984 and 1988 La Niña). This demonstrates that there are years other than ENSO extremes that contribute to the TBO.

To address the contribution of ENSO versus non-ENSO onset years to the TBO in the Australian monsoon, a similar SVD calculation to that in Fig. 12 is performed without the ENSO onset years (not shown). As in the Indian monsoon non-ENSO onset years, there are very similar patterns to that for the full set of years, with pattern correlations for Pacific SSTs (Fig. 12c) of +0.89, with monsoon rainfall associated with Pacific SSTs (Fig. 12d) of +0.53, pattern correlations for southeast Asian precipitation (Fig. 12e) of +0.72, and with monsoon rainfall associated with southeast Asian precipitation (Fig. 12f) of +0.68. Also similar to the Indian monsoon, The Indian Ocean SST relationships are not as strong for all years and non-ENSO onset years with pattern correlations for Indian SSTs (Fig. 12a) of +0.53, and with subsequent Australian monsoon rainfall (Fig. 12b) of +0.41. Also, as in the Indian monsoon non-ENSO onset years, the maximum positive SST values for SON are centered more in the southeastern part of the domain (not shown). Thus, ENSO onset years are tied strongly to the dipole pattern in SON, but non-ENSO onset years are not so strongly linked.

6. Time evolution

To examine the time evolution of the conditions associated with the TBO, we regress the precipitation SVD expansion coefficient time series computed for JJAS precipitation and MAM 500-hPa height (patterns in Figs. 8a,b), and JJAS precipitation and Indian Ocean SST (patterns in Figs. 8c,d) against precipitation, surface wind, and surface temperature data for seasons depicted in Fig. 3 and results are shown in Figs. 14 and 15, respectively. It was noted that Indian and Pacific SST SVD patterns for all years are similar, so only the Indian Ocean SST SVD association with JJAS precipitation is used here.

The JJAS Indian monsoon precipitation SVD expansion coefficient time series derived for MAM 500-hPa height anomalies over Asia regressed against surface wind, surface temperature, and precipitation is shown in Fig. 14. If only values exceeding a 95% significance level were plotted, the number of vectors and contours would be reduced. However, we choose to plot values at every grid point since the time series are relatively short and we wish to address the physical significance of the plotted quantities (Nicholls 2001).

Note that the sign and pattern for JJAS precipitation in Fig. 14e closely resembles the sign and pattern in Fig. 8b (as it must since they are derived from the same expansion coefficient time series, with the heterogeneous association in Fig. 8 and homogeneous in Fig. 14), with enhanced precipitation over much of northern India, Bangladesh, and Burma. Also note that the surface temperature regressions in Fig. 14d for MAM (with warm conditions over much of Asia) are comparable in terms of sign and pattern to Fig. 9. This shows that the sign convention of the regressions in Fig. 14 is consistent with the physical interpretation of Figs. 8 and 9.

Conditions leading up to the precipitation pattern in Fig. 14e can be seen to involve a positive precipitation maximum with regression values of over 0.3 mm day^{-1} over the equatorial western Pacific Ocean near 150°E to the date line in the DJF-1 (Fig. 14a). As in Fig. 4 for the simultaneous associations, positive values extend over northern Australia, but also reach farther west over Papua New Guinea in association with westerly wind anomalies there. In fact the precipitation is enhanced far enough west that the regressed SST pattern in Fig. 14b shows negative anomalies in the eastern equatorial Pacific opposite to that in the idealized schematic in Fig. 3.

There is suppressed precipitation over Malaysia and the Indian Ocean, with regression values of several tenths of a mm day^{-1}. Though this is two seasons removed from the SVD calculation for JJAS, this pattern also resembles the contemporaneous SVD for DJF in Fig. 4. This indicates that the associations in a given season and the relationships to following seasons are robust.

The pattern of convective heating anomalies stretching from eastern Africa to the western equatorial Pacific was noted earlier to be associated with an anomalous ridge of positive 500-hPa height anomalies over Asia, and warmer Asian land temperatures. Similarly, anomalously warm land temperatures with regression values of greater than +0.5°C appear over much of south Asia in DJF-1 (Fig. 14b) as was noted for the contemporaneous relationship in Fig. 7. In association with the

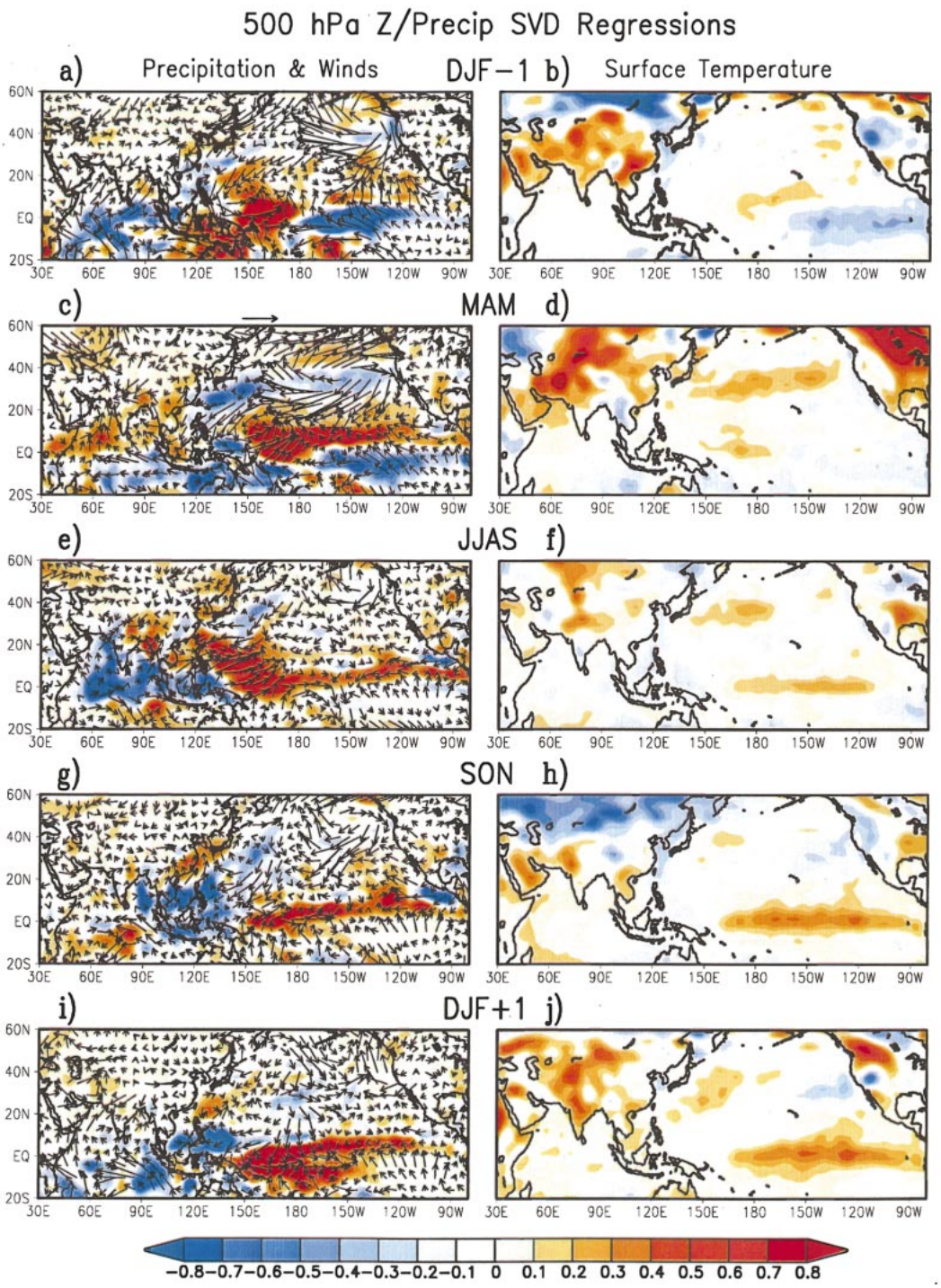

FIG. 14. The JJAS Indian monsoon precipitation SVD expansion coefficient time series derived from MAM 500-hPa height anomalies over Asia (pattern in Fig. 8b) regressed against surface wind, precipitation, and surface temperature for seasons lagging and leading the Indian monsoon. Units are in m s^{-1}, mm day^{-1}, and °C (unit std dev of the expansion coefficient of the first JJAS precipitation vector for surface wind, precipitation, and surface temperature, respectively)$^{-1}$. Scaling vector above part (c) is 0.75 m s^{-1}. (a) Precipitation and winds for DJF prior to the Indian monsoon; (b) surface temperature for DJF prior to the Indian monsoon; (c) precipitation and winds for MAM prior to the Indian monsoon; (d) surface temperature for MAM prior to the Indian monsoon; (e) precipitation and winds for JJAS Indian monsoon season; (f) surface temperature for JJAS Indian monsoon season; (g) precipitation and winds for SON after the Indian monsoon; (h) surface temperature for SON after the Indian monsoon; (i) precipitation and winds for DJF after the Indian monsoon; (j) surface temperature for DJF after the Indian monsoon.

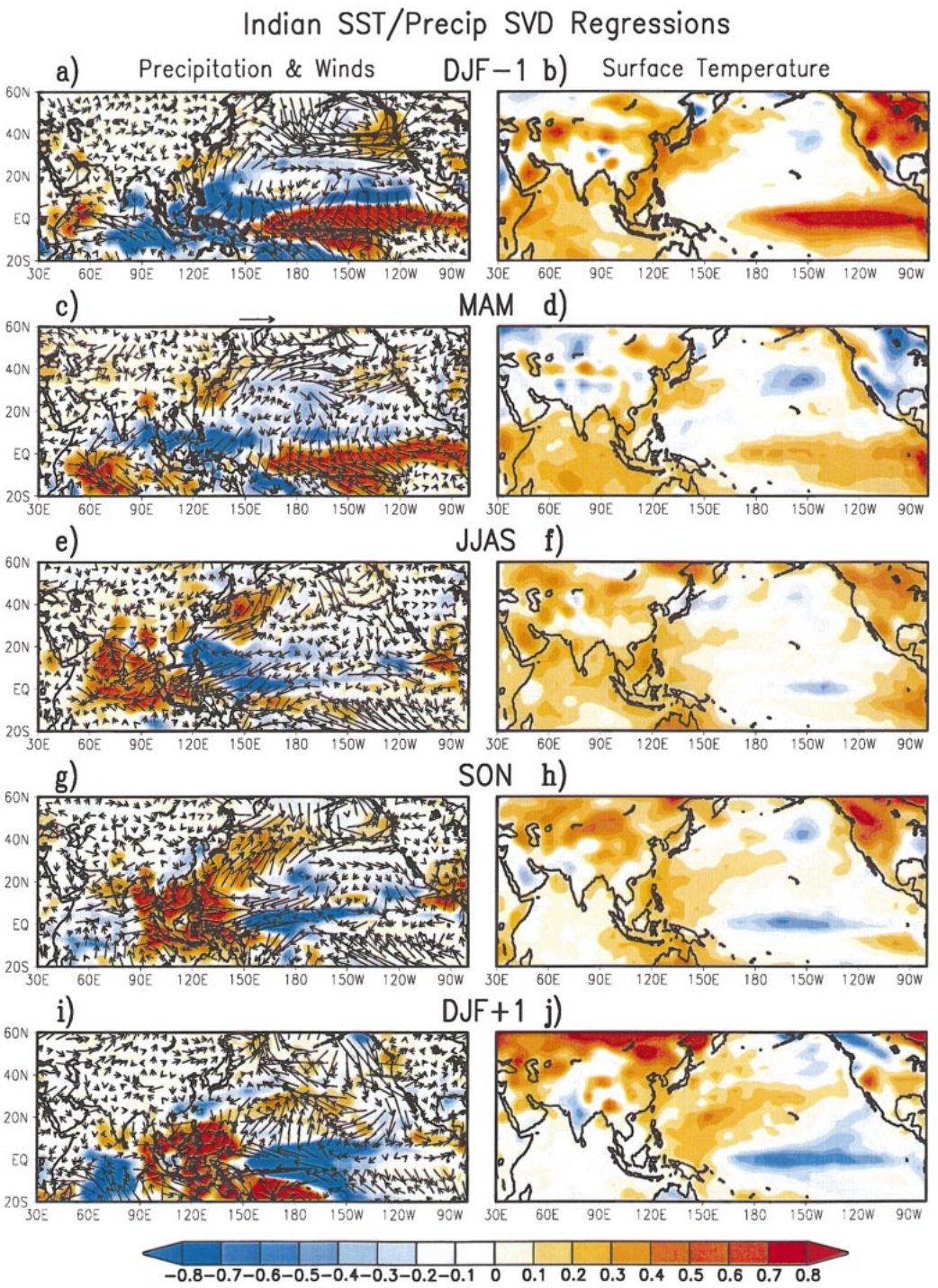

FIG. 15. The JJAS Indian monsoon precipitation SVD expansion coefficient time series derived from MAM Indian Ocean region surface temperature (pattern in Fig. 8d) regressed against surface wind, precipitation, and surface temperature for seasons lagging and leading the Indian monsoon. Units are in m s^{-1}, mm day^{-1}, and °C (unit std dev of the expansion coefficient of the first JJAS precipitation vector for surface wind, precipitation, and surface temperature, respectively)$^{-1}$. Scaling vector above part (c) is 0.75 m s^{-1}. (a) Precipitation and winds for DJF prior to the Indian monsoon; (b) surface temperature for DJF prior to the Indian monsoon; (c) precipitation and winds for MAM prior to the Indian monsoon; (d) surface temperature for MAM prior to the Indian monsoon; (e) precipitation and winds for JJAS Indian monsoon season; (f) surface temperature for JJAS Indian monsoon season; (g) precipitation and winds for SON after the Indian monsoon; (h) surface temperature for SON after the Indian monsoon; (i) precipitation and winds for DJF after the Indian monsoon; (j) surface temperature for DJF after the Indian monsoon.

precipitation anomalies, there are westerly wind anomalies of about +0.5 m s^{-1} in the western Pacific, and southeasterly anomalies over the equatorial Indian Ocean.

In MAM (Fig. 14c) the lagged pattern of regressed tropical precipitation anomalies is similar to the simultaneous SVD calculation in Fig. 6b. There are enhanced precipitation regression values of several tenths of a mm day^{-1} over the western Indian Ocean and parts of Indochina, and larger values of greater than +0.6 mm day^{-1} in the western Pacific east of about 160°E (see Ju and Slingo 1995). There is suppressed precipitation north of Papua New Guinea, with regression values of several tenths of a mm day^{-1}. Similarly, this tropical precipitation pattern is associated with positive 500-hPa height anomalies over Asia (Fig. 8a) and anomalously warm Asian land temperatures with regression values greater than +0.7°C (Fig. 14d) similar to those for the contemporaneous relationship in Fig. 7. Both have an enhanced surface temperature gradient over south Asia. Anomalous westerly wind regression values of about +0.3 m s^{-1} continue over the western equatorial Pacific with southwesterly values of about that same magnitude over the Arabian Sea, and easterly anomaly winds of about 0.5 m s^{-1} along the equator in the western Indian Ocean.

The JJAS patterns in Figs. 14e,f show enhanced precipitation over northeastern India and Bangladesh as noted above with strengthened southwesterly flow over the Arabian Sea. In addition, there is suppressed precipitation over the Indian Ocean, eastern Asia, Malaysia, and parts of Indonesia, while there is enhanced precipitation over Japan, the western Pacific northeast of the Philippines, and along the ITCZ in the Pacific. This enhanced precipitation component has almost a hemispheric ITCZ-like aspect with a band of positive precipitation regression values extending from India across the South China Sea and east of the Philippines. There are strengthened south and southwest winds across the Arabian Sea with regression values of about 0.3 m s^{-1}, and westerly anomalies of about twice that magnitude in the western tropical Pacific. SSTs in the central equatorial Pacific are anomalously warm but with small regression values of about +0.2, while SSTs in the northern Indian Ocean are anomalously cool.

The SON season in Figs. 14g,h shows positive precipitation regression values of roughly +0.4 mm day^{-1} over eastern China and north of the equator in the Pacific, easterly regression values of about 0.5 m s^{-1} in the equatorial eastern Indian Ocean, and westerly anomalies of about that same magnitude near the date line in the Pacific associated with small positive SST regression values of +0.4°C in the central and eastern tropical Pacific. There is the suggestion of a weak positive dipole of SSTs and easterly wind anomalies across the equatorial Indian Ocean, with somewhat warmer SSTs in the west and cooler in the east. By DJF following the monsoon (Figs. 14i,j), there are easterly anomaly winds in the far western equatorial Pacific, easterly anomaly winds south of the equator in the Indian Ocean, and a mixture of positive and negative precipitation anomalies in the Australian monsoon region.

The lagged precipitation, wind, and SST regressions in Fig. 14 are consistent with the simultaneous calculations for DJF and MAM in Figs. 4–7 but differ in some respects with the hypothesized evolution in Fig. 3. This suggests that the enhanced meridional temperature gradient mechanism depicted in Fig. 14 may not work in concert with the SST-driven ones. To explore the latter in Fig. 15, the SVD expansion coefficient time series from the JJAS Indian monsoon rainfall calculated using the MAM Indian SST in Figs. 8c,d are regressed against surface winds, temperatures, and precipitation. Figure 8d can be compared to be similar (as it must be, as noted for Fig. 14e) with a comparable sign convection to Fig. 15e. But the larger domain is seen to show enhanced precipitation not only over parts of southern India and Bangladesh as was seen in Fig. 8d, but also over much of the Indian Ocean region as well with regression values greater than +0.4 mm day^{-1}. The Indian Ocean SST anomalies in MAM are positive with largest values south of about 10°N in Fig. 15d. The anomalously warm SSTs over the Indian Ocean in MAM (Fig. 15d) are comparable to the values shown in Fig. 8c.

The DJF preceding the Indian monsoon shows a weak Australian monsoon with negative precipitation regression values of at least −0.6 mm day^{-1} over almost the entire Australian monsoon domain in Fig. 15a, with easterly anomaly wind regression values of around 0.7 m s^{-1} along the equatorial Indian Ocean with somewhat weaker easterly anomalies in the far western equatorial Pacific. There are also westerly anomaly wind regression values of nearly 0.8 m s^{-1} associated with anomalously warm SSTs in the eastern and central equatorial Pacific (Fig. 15b). In MAM there is suppressed precipitation (roughly −0.4 mm day^{-1}) near 10°N stretching from East Africa to about 120°W, while northeasterly anomaly wind regression values of about 0.4 m s^{-1} continue in the western equatorial Pacific and westerly anomaly winds appear in the far western equatorial Indian Ocean (Fig. 15c). The Indian Ocean is anomalously warm as is the central and eastern equatorial Pacific (Fig. 15d) with regression values of greater than 0.4°C. There is little consistent surface temperature anomaly pattern over southern Asia.

As noted above, in JJAS (Fig. 15e) there is enhanced precipitation over most of India, Bangladesh, and the Indian Ocean (some regression values exceed +0.8 mm day^{-1}). Since most of the anomalous precipitation lies over the Indian Ocean in Fig. 15e, the main anomalous surface wind convergence is near the equator in the Indian Ocean, with anomalous westerly regression values of about 0.4 m s^{-1} in the western Indian Ocean, and anomalous easterlies with regression values of around 0.5 m s^{-1} in the eastern Indian Ocean stretching

across most of Southeast Asia into the western Pacific Ocean. Even though there is enhanced Indian monsoon rainfall in Fig. 15e, there are easterly wind anomalies over the Arabian Sea where one would expect to see southwesterly anomalies with stronger inflow as in Fig. 14e. To examine this response, GCM sensitivity experiments with specified SST anomalies over the Indian Ocean show that greater precipitation over the Indian Ocean has a regional effect on winds that can produce easterly anomalies over the Arabian Sea even with enhanced rainfall over India (MEAR1).

In Fig. 15f, SSTs have transitioned from positive in MAM to negative in JJAS in the central equatorial Pacific and small negative SST anomalies have just appeared off the coast of equatorial Africa in the western Indian Ocean in association with the implied enhanced upwelling from the westerly wind anomalies there.

In SON (Figs. 15g,h) the strong monsoon convective maximum from JJAS traverses east and south encountering anomalously warm SSTs in its path and covers most of Southeast Asia with positive precipitation anomalies with regression values mostly greater than $+0.7$ mm day^{-1}. There is surface wind convergence associated with that convective maximum, with westerly anomalies over much of the equatorial Indian Ocean, and easterly anomalies over the western Pacific, both with regression values of greater than 0.5 m s^{-1}. A negative SST dipole in the Indian Ocean has small negative anomalies in the west and positive anomalies in the east, and there are strengthening negative SST regression values in the equatorial central Pacific of roughly -0.5°C.

By DJF+1 after the Indian monsoon, the strong convective maximum (with regression values mostly greater than 0.7 mm day^{-1}) has become established over most of the Australian monsoon domain (Fig. 15i) and westerly anomaly winds with regression values of greater than 0.5 m s^{-1} now shifted south of the equator in the tropical southeastern Indian Ocean. There is evidence of westerly anomaly wind regression values of about 0.3 m s^{-1} in the far western equatorial Pacific with easterly anomaly wind regression values of about 0.7 m s^{-1} east of 150°E. As mentioned earlier, this seasonal evolution is similar for the Pacific SVD projection for all years (not shown) indicating that the Indian and Pacific are linked in many years through large-scale east–west atmospheric circulation anomalies (the WWC and EWC) associated with the movement of the convective maximum from the Indian to Australian monsoon, and its coupled interactions with the ocean.

In comparing the sequences depicted in Figs. 14 and 15 with the idealized evolution of the TBO in Fig. 3, a number of interesting aspects emerge. First, for the linkages between the tropical convective heating anomalies, 500-hPa circulation, and land temperature anomalies, there are differences in the connections to the tropical Pacific. This also relates to where, exactly, precipitation anomalies occur over the south Asian monsoon region. The apparent contribution of anomalous meridional temperature gradients prior to the Indian monsoon associated with tropical convective heating anomalies is mainly related to enhanced precipitation over some land areas of south Asia (northeast India, Bangladesh, and Burma). They apparently can act independently from forcing from the tropical Pacific since the sense of the evolution of SST anomalies in the tropical Pacific is opposite between Figs. 14 and 15. This is not a result of a random choice of sign convention since, as noted above, the sign of the patterns in Figs. 14 and 15 match those of the SVD patterns in Figs. 4–8 for consistent physical interpretation. Additionally, the Asian land temperature anomalies in Fig. 14 are not biennial, with positive land temperature anomalies in DJF-1 and DJF+1. However, since the two sequences presumably represent components of the actual evolution and are not orthogonal, there is overlap as could be expected from such a coupled system. In any given year in the TBO one or the other of the processes can contribute to the actual patterns of rainfall as seen in Fig. 10a. Since the more land-based precipitation pattern in Fig. 14e and the Indian Ocean–based pattern in Fig. 15e are associated with different evolutions of Pacific SSTs, it is no surprise that in any given monsoon year the linkage with the tropical Pacific can be intermittent.

The question still remains concerning whether the land-based meridional temperature gradient mechanism or the SST-based mechanisms could, independently, produce the precipitation anomaly patterns in the lagged regression plots in Figs. 14 and 15. This question is addressed directly through the use of GCM sensitivity experiments by MEAR1. Results show that indeed each mechanism can produce comparable patterns of precipitation response in Figs. 14 and 15, and that the SST-based mechanisms are relatively stronger. Yet, as shown in Figs. 10 and 13, each mechanism can make partial contributions in any given year.

In any case, the circulation-related sequence in Fig. 14 appears to produce a more anomalous hemispheric precipitation pattern during the monsoon season, with the Indian monsoon enhancement part of an ITCZ-like positive precipitation anomaly pattern stretching east of the Philippines. However, the more Indian Ocean–based precipitation anomaly pattern in Fig. 15e has an east–west character, with enhanced precipitation over most of the Indian sector and suppressed precipitation over the western Pacific east of the Philippines. This strong convective maximum in the Indian sector then progresses in Fig. 15 much as depicted in Fig. 3, remaining strong in its southeastward progression across Southeast Asia in SON culminating in a strong Australian monsoon in the following DJF. Conversely, the meridional temperature gradient pattern shows more of an overall weakened convective maximum progressing southeastward with the seasonal cycle as indicated by the negative precipitation regression values in that region.

It is also clear from the surface winds that there are

ocean dynamical linkages. Anomalous winds in the far western equatorial Pacific in DJF in Fig. 15 precede transitions of SSTs in the central and eastern equatorial Pacific, with the transition starting in MAM and opposite sign SST anomalies becoming established in JJAS. Thus a preliminary answer to the question of ''what makes the TBO flip from one year to the next'' directly involves coupled ocean–atmosphere interaction in the Australian monsoon region in DJF, which would trigger oceanic Kelvin waves that affect the thermocline farther east in the Pacific to induce an SST transition in subsequent months. In addition, surface wind anomalies in the equatorial Indian Ocean are seen to initiate the Indian Ocean SST dipole pattern starting half a year later in JJAS, peaking in SON, and making the full transition to opposite sign anomalies by the subsequent DJF. We directly address the question of ocean dynamics in Meehl et al. (2002, manuscript submitted to *J. Climate*). In that paper we examine composites of TBO transitions in observed atmospheric and upper-ocean data, and show that oceanic Rossby waves (Webster et al. 1999) also play a role in these transitions. Loschnigg et al. (2002, manuscript submitted to *J. Climate*) show similar results from an analysis of a global coupled model.

7. Discussion and conclusions

In Fig. 3 we presented a hypothesized series of coupled interactions to account for conditions associated with TBO transitions. The various contemporaneous and lagged SVD and composite analyses have raised some interesting issues. First, due to the well-known seasonal persistence from Indian to Australian monsoon, the most important TBO transitions occur from MAM to JJAS. Those transitions account first for the interannual variations of the patterns of monsoon rainfall in JJAS, and then for a majority of years of Australian monsoon rainfall strength. However, the JJAS rainfall over Australasia, that is dynamically important for the large-scale climate system in the Indian and Pacific sectors, covers a huge area of land and ocean. In this context, the Indian monsoon, strictly over India and more broadly interpreted as rainfall over south Asian land areas, is only on the northwestern edge of the vast maximum of JJAS rainfall that extends over much of the tropical Indian Ocean and east to Southeast Asia. Any analysis of the dynamically important mechanisms must account for variations in this entire pattern, not just small regional pieces of it. We saw that the regional pieces (such as India) have rainfall that is influenced by conditions and associated rainfall anomalies over much larger regions.

For the tropical Pacific and Indian Ocean conditions, it was noted that the SST transitions start to occur two seasons later in the Indian Ocean in conjunction with the Indian monsoon (JJAS) compared to the central and eastern Pacific which begins the transition process in association with the Australian monsoon (DJF). In the Pacific the SST transition is complete by the following Indian monsoon in JJAS, and finishes in the Indian Ocean by the following Australian monsoon in DJF. This is due to the nature of the coupled wind forcing and ocean dynamical response along with the seasonal evolution of the convective maximum as it traverses from the Indian region to the Australian region. As part of this seasonal evolution and associated coupled wind forcing, in conjunction with ocean dynamics, the SST dipole in the Indian Ocean starts to appear as part of this transition in the Indian Ocean in JJAS. The SST transition is part way completed in SON when the Indian Ocean SST dipole is most apparent, and is fully transitioned by DJF when the dipole gives way to SST anomalies in the tropical Indian Ocean of one sign and the influence of the Australian monsoon is most evident. There is a linkage between the Indian and Pacific Oceans due to the coupling inherent in the large-scale east–west atmospheric circulations (the WWC and EWC) associated with the seasonal movement of the convective maximum over Australasia, but with the 6-month lags involved with the seasonal cycle and coupled atmosphere–ocean interactions. These linkages account for much of the rainfall variability over the tropical Indian Ocean, and parts of western India, Bangladesh, and eastern China (Figs. 8, 15). *The dynamical interactions responsible for SST transitions in the Indian Ocean begin with the Indian monsoon and end with the subsequent Australian monsoon. In the Pacific SST transitions begin with the Australian monsoon and end with the following Indian monsoon.* The Indian and Pacific Oceans thus have a certain seasonal symmetry with the SST transitions occurring half a year apart.

It has been noted that the influence of the tropical Pacific SST anomalies on Indian monsoon rainfall has diminished since the late 1970s (Krishna Kumar et al. 1999). Other changes in base state apparently have occurred in the Indian Ocean to alter certain monsoon linkages with conditions such as SST (Clark et al. 2000). Since our data only cover the period since this apparent change, we note that both the Indian and Pacific SVD patterns are similar (Fig. 8) with a greater link to rainfall over the Indian Ocean with peripheral (but regionally important) influences over India and other south Asian land areas. The importance of the Indian Ocean SSTs to subsequent patterns of Indian monsoon rainfall was indicated by the fact that the squared covariance accounted for was 58% for the MAM Indian SST/JJAS monsoon rainfall SVD association, but only 39% for each of the Pacific and 500-hPa height associations (Fig. 8). Part of the reason for the somewhat reduced amplitude for the Pacific SSTs is that there is an implied transition from MAM to JJAS in the Pacific that reduces seasonal persistence, while in the Indian Ocean the sign of SST anomalies is mostly the same from MAM to JJAS, with the transition occurring over the next two seasons as part of the SST dipole.

It was also noted that the rainfall over the Indian

Ocean, in particular, affects to a great extent the low-level wind anomalies over the equator and the appearance of the Indian Ocean SST dipole in the equatorial Indian Ocean. We speculate that in other time periods this may have been more important for land precipitation if the details of the SST base states were different so as to change where the SST anomalies have their greatest influence on precipitation.

There is another important effect on JJAS monsoon transitions, and that is anomalous meridional temperature gradients over Asia. An enhancement of the meridional temperature gradient was seen to contribute to stronger JJAS monsoon rainfall mainly over land areas of northeast India, Burma, Vietnam, and ocean areas east of the Philippines (Figs. 8 and 14). Interestingly, there is an opposite relationship with tropical Pacific SSTs compared to the Indian and Pacific conditions. That is, enhanced south Asian land precipitation can occur with weak warming of SSTs in the central Pacific in the SVD regressions (Fig. 14), while enhanced rainfall over large areas of the Indian Ocean as well as some south Asian land areas occurs with cooling of SSTs in the central Pacific (Fig. 15).

The anomalous meridional temperature gradients over Asia in seasons prior to the south Asian monsoon are seen to be related to convective heating anomalies in the tropical Indian and far western Pacific Oceans, associated with SST anomalies in those regions (Figs. 4, 5, 14). These convective heating anomaly patterns are not that far removed from the inverse pattern associated with the Indian and Pacific conditions (Fig. 15). Subtle shifts in the forcing from the Tropics can make a difference in the midlatitude response and associated meridional temperature gradients (cf. Figs. 14 and 15). Thus the anomalous meridional temperature gradient condition can disrupt the connection with ENSO and monsoon strength, and contribute to the ''intermittent'' nature of that connection (e.g., Webster and Yang 1992).

Such intermittent connections dictate that some kind of approach be used to separate the different conditions associated with TBO transitions. The SVD and cumulative pattern correlation techniques used in this paper are one approach. In this way the magnitude of the associations of the different transition conditions can be quantified each year in terms of pattern, and can also be used to derive information on monsoon strength in terms of the reconstructed area-averaged precipitation indices.

It was hypothesized earlier that various conditions in seasons prior to the monsoons are associated with interannual transitions or flip-flops, and this has been demonstrated with these analyses. Coupled dynamical interactions involving atmosphere and ocean are necessary to sustain such interannual transitions, with the phasing of the transitions in each ocean dependent on the seasonal cycle of convection in the respective regions. Thus anomalous Australian monsoon rainfall in DJF and associated surface wind anomalies in the far western equatorial Pacific could trigger oceanic Kelvin waves that contribute to the Pacific SST transition a season later in MAM. Likewise, anomalous monsoon rainfall and surface wind anomalies in the tropical Indian Ocean during JJAS could contribute to the Indian Ocean SST dipole in SON, with the dipole transitioning to SST anomalies of all one sign by DJF in association with the anomalous surface wind forcing connected with the Australian monsoon to the east. Simultaneously, surface wind anomalies to the east of the Australian monsoon in the far western equatorial Pacific then start acting on the Pacific Ocean to initiate the subsequent transition there in MAM, and so on. Therefore, the coupled processes in the Indian Ocean do not occur simultaneously with those in the Pacific, but they are linked through the Asian–Australian monsoon evolutions. Previous studies have pointed to the role of surface wind forcing in the western equatorial Pacific (Lau and Wu 2001; Kim and Lau 2001; Clarke et al. 1998; Clarke and Shu 2000; Chung and Nigam 1999) and equatorial Indian Ocean (Clarke et al. 1998; Reason et al. 2000; Saji et al. 1999; Webster et al. 1999). Here we place these forcings in the framework of the TBO evolution involving dynamical coupled interactions across the Indian and Pacific sectors. The upper-ocean heat content anomalies that are a consequence contribute to the persistence of SST anomalies that are crucial for the convective heating anomalies and maintenance of the large-scale east–west circulation in the atmosphere (the WWC and EWC) during the TBO in Indian and Pacific Oceans (Meehl 1993). Details of the coupled ocean dynamics involved with these transitions are explored by Meehl et al. (2002, manuscript submitted to *J. Climate*).

It has often been asked if there would be a TBO (or ENSO) without the Indian Ocean. It is likely that the large-scale tropical Pacific transition condition would still contribute to TBO/ENSO variability associated with the Asian–Australian monsoon. Additionally, the meridional temperature gradient condition could also contribute as noted in Fig. 10. However, it was also documented in Fig. 10 that, in a number of years, MAM Indian Ocean SSTs are associated with Indian monsoon rainfall independent from the other conditions. GCM experiments have demonstrated that the Indian Ocean by itself can cause enhanced south Asian monsoon rainfall (MEAR1). Therefore, the implication is that without the regional influence of Indian Ocean SSTs, the system would be less biennial. This was demonstrated in the model experiments of Kim and Lau (2001) where additional wind forcing in the far western Pacific, implied to be tied to monsoon processes, made the Pacific basin SSTs more biennial.

To take that idea one step further, it has been observed that there are epochs when either the TBO or ENSO components are stronger than in others (e.g., Webster et al. 1998; Torrence and Webster 1999). Results presented here suggest that if one or more of the TBO transition conditions make less of a contribution during

some period of time, it follows that the system would be less biennial with more power shifted to lower frequencies. Conversely, if all the transition conditions are working during some time period, it is likely that the system would be more biennial with less power at lower frequencies. To test that speculation, carefully designed coupled model experiments with certain ocean or land conditions specified would be necessary. Such experiments are currently being formulated.

Two questions were posed earlier that we can provide tentative answers for:

1) What makes the system flip-flop? It is the combination of large-scale and/or regional conditions in seasons prior to the monsoon, set up by coupled air–sea–land interactions the previous year, that result in a transition to a relatively strong or weak monsoon compared to the previous year.

2) Why is MAM season critical for these transitions? It involves geography and the seasonal cycle of convection. When the convective maximum reaches the Australian monsoon in DJF, being either reinforced by warm SSTs or weakened by cold SSTs set up the previous year, anomalous convection is associated with surface wind anomalies in the tropical western Pacific that induce an ocean dynamical response that, a season later, begins to affect SSTs across the Pacific. By JJAS, SST anomalies are set up across the Pacific when the convective maximum is over south Asia. Meanwhile, regional coupled interactions involved with Indian SSTs and circulation/temperature anomalies over Asia, set up by conditions the previous year, can result in a transition in the TBO as well. Once the sense of the large-scale east–west atmospheric circulation (the WWC and EWC) is set in JJAS, the Indian Ocean SST dipole transition begins. The convective maximum retains seasonal persistent as it moves from the Indian to Australian monsoons to culminate in a full Indian Ocean SST transition by the following Australian monsoon in DJF. This then sets the SST transition in the Pacific in motion due to the coupled wind anomalies in the far western equatorial Pacific associated with the anomalous state of the Australian monsoon, and so on. The unique geography of the Indian–Pacific region dictates that, in the climatological seasonal cycle, the convective maximum retains continuity as it progresses from the Indian to Australian monsoons but not on the return (Meehl 1987, his Fig. 3). This aspect of the seasonal cycle is manifested in year-to-year variability of the coupled system over this large region.

It was noted earlier that use of first SVD modes does not guarantee orthogonality and, in fact, it was shown that all the transition conditions, particularly Indian and Pacific SSTs, are related. The single and cumulative pattern correlation technique is then used to quantify the separate contributions of the transition conditions year by year. GCM sensitivity experiments have shown that the forcings from the transition conditions can, by themselves, produce patterns similar to those seen in the first component SVDs in this paper (MEAR1). This indicates that the SVD patterns are not statistical artifacts and do have physical significance, thus helping to quantify TBO processes.

Acknowledgments. A portion of this study was supported by the Office of Biological and Environmental Research, U.S. Department of Energy, as part of its Climate Change Prediction Program. The authors thank Johannes Loschnigg and an anonymous reviewer for helpful comments on the manuscript.

REFERENCES

Allan, R. J., and R. D. D'Arrigo, 1999: 'Persistent' ENSO sequences: How unusual was the 1990–95 El Nino? *Holocene,* **9,** 101–118.

Bamzai, A., and J. Shukla, 1999: Relation between Eurasian snow cover, snow depth and the Indian summer monsoon: An observational study. *J. Climate,* **12,** 3117–3132.

Chang, C. P., and T. Li, 2000: A theory for the tropical tropospheric biennial oscillation. *J. Atmos. Sci.,* **57,** 2209–2224.

Chung, C., and S. Nigam, 1999: Asian summer monsoon—ENSO feedback on the Cane–Zebiak model ENSO. *J. Climate,* **12,** 2787–2807.

Clark, C. O., J. E. Cole, and P. J. Webster, 2000: Indian Ocean SST and Indian summer rainfall: Predictive relationships and their decadal variability. *J. Climate,* **13,** 2503–2519.

Clarke, A. J., and L. Shu, 2000: Quasi-biennial winds in the far western equatorial Pacific phase-locking El Niño to the seasonal cycle. *Geophys. Res. Lett.,* **27,** 771–774.

——, X. Liu, and S. van Gorder, 1998: Dynamics of the biennial oscillation in the equatorial Indian and far western Pacific Oceans. *J. Climate,* **11,** 987–1001.

Goswami, B. N., 1995: A multiscale interaction model for the origin of the tropospheric QBO. *J. Climate,* **8,** 524–534.

Iizuka, S., T. Matsuura, and T. Yamagata, 2000: The Indian Ocean SST dipole simulated in a coupled general circulation model. *Geophys. Res. Lett.,* **27,** 3369–3372.

Jin, F.-F., J. D. Neelin, and M. Ghil, 1994: El Niño on the Devil's Staircase: Annual subharmonic steps to chaos. *Science,* **264,** 70–72.

Ju, J., and J. Slingo, 1995: The Asian summer monsoon and ENSO. *Quart. J. Roy. Meteor. Soc.,* **121,** 1133–1168.

Kalnay, E., and Coauthors,1996: The NCEP/NCAR 40-Year Reanalysis Project. *Bull. Amer. Meteor. Soc.,* **77,** 437–471.

Kawamura, R., 1998: A possible mechanism of the Asian summer monsoon–ENSO coupling. *J. Meteor. Soc. Japan,* **76,** 1009–1027.

Kiladis, G. N., and H. van Loon, 1988: The Southern Oscillation. Part VII: Meteorological anomalies over the Indian and Pacific sectors associated with the extremes of the oscillation. *Mon. Wea. Rev.,* **116,** 120–136.

——, and H. F. Diaz, 1989: Global climatic anomalies associated with extremes in the Southern Oscillation. *J. Climate,* **2,** 1069–1090.

Kim, K.-M., and K.-M. Lau, 2001: Dynamics of monsoon-induced biennial variability in ENSO. *Geophys. Res. Lett.,* **28,** 315–318.

Kripalani, R. H., and A. Kulkarni, 1999: Climatology and variability of historical Soviet snow depth data: Some new perspectives in snow–Indian monsoon teleconnections. *Climate Dyn.,* **15,** 475–489.

Krishna Kumar, K., B. Rajagopalan, and M. A. Cane, 1999: On the weakening relationship between the Indian monsoon and ENSO. *Science,* **284,** 2156–2159.

Lau, K. M., and S. Yang, 1996: The Asian monsoon and predictability of the tropical ocean–atmosphere system. *Quart. J. Roy. Meteor. Soc.,* **122,** 945–957.

——, and H.-T. Wu, 1999: Assessment of the impacts of the 1997–98 El Niño on the Asian–Australia monsoon. *Geophys. Res. Lett.,* **26,** 1747–1750.

——, and ——, 2001: Principal modes of rainfall–SST variability of the Asian summer monsoon: A reassessment of the monsoon–ENSO relationship. *J. Climate,* **14,** 2880–2895.

Li, C., and M. Yanai, 1996: The onset and interannual variability of the Asian summer monsoon in relation to land–sea thermal contrast. *J. Climate,* **9,** 358–375.

Loschnigg, J., and P. J. Webster, 2000: A coupled ocean–atmosphere system of SST modulation for the Indian Ocean. *J. Climate,* **13,** 3342–3360.

Madden, R. A., and R. H. Jones, 2001: A quantitative estimate of the effect of aliasing in climatological time series. *J. Climate,* **14,** 3987–3993.

Meehl, G. A., 1987: The annual cycle and interannual variability in the tropical Indian and Pacific Ocean regions. *Mon. Wea. Rev.,* **115,** 27–50.

——, 1993: A coupled air–sea biennial mechanism in the tropical Indian and Pacific regions: Role of the ocean. *J. Climate,* **6,** 31–41.

——, 1994: Coupled land–ocean–atmosphere processes and south Asian monsoon variability. *Science,* **266,** 263–267.

——, 1997: The south Asian monsoon and the tropospheric biennial oscillation. *J. Climate,* **10,** 1921–1943.

——, and J. M. Arblaster, 2001a: Indian monsoon GCM sensitivity experiments testing tropospheric biennial oscillation transition conditions. *J. Climate,* in press.

——, and ——, 2001b: The tropospheric biennial oscillation and Indian monsoon rainfall. *Geophys. Res. Lett.,* **28,** 1731–1734.

Nicholls, N., 2001: The insignificance of significance testing. *Bull. Amer. Meteor. Soc.,* **82,** 981–986.

Ogasawara, N., A. Kitoh, T. Yasunari, and A. Noda, 1999: Tropospheric biennial oscillation of the ENSO-monsoon system in the MRI coupled GCM. *J. Meteor. Soc. Japan,* **77,** 1247–1270.

Rao, K. G., and B. N. Goswami, 1988: Interannual variations of the sea-surface temperature over the Arabian Sea and the Indian monsoon: A new perspective. *Mon. Wea. Rev.,* **116,** 558–568.

Rasmusson, E. M., and T. H. Carpenter, 1983: The relationship between eastern equatorial Pacific sea surface temperatures and rainfall over India and Sri Lanka. *Mon. Wea. Rev.,* **111,** 517–528.

Reason, C. J. C., R. J. Allan, J. A. Lindesay, and T. J. Ansell, 2000: ENSO and climatic signals across the Indian Ocean basin in the global context: Part 1. Interannual composite patterns. *Int. J. Climatol.,* **20,** 1285–1327.

Ropelewski, C. F., M. S. Halpert, and X. Wang, 1992: Observed tropospheric biennial variability and its relationship to the Southern Oscillation. *J. Climate,* **5,** 594–614.

Saji, N. H., B. N. Goswami, P. N. Vinayachandran, and T. Yamagata, 1999: A dipole mode in the tropical Indian Ocean. *Nature,* **401,** 360–363.

Shukla, J., and D. A. Paolino, 1983: The Southern Oscillation and long-range forecasting of the summer monsoon rainfall over India. *Mon. Wea. Rev.,* **111,** 1830–1837.

Tomita, T., and T. Yasunari, 1996: Role of the northeast winter monsoon on the biennial oscillation of the ENSO/monsoon system. *J. Meteor. Soc. Japan,* **74,** 399–413.

Torrence, C., and P. J. Webster, 1999: Interdecadal changes in the ENSO-monsoon system. *J. Climate,* **12,** 2679–2690.

Trenberth, K. E., 1999: Atmospheric moisture recycling: Role of advection and local evaporation. *J. Climate,* **12,** 1368–1381.

——, D. P. Stepaniak, and J. W. Hurrell, 2001: Quality of reanalyses in the Tropics. *J. Climate,* **14,** 1499–1510.

Webster, P. J., and S. Yang, 1992: Monsoon and ENSO: Selectively interactive systems. *Quart. J. Roy. Meteor. Soc.,* **118,** 877–926.

——, V. O. Magana, T. N. Palmer, J. Shukla, R. A. Tomas, M. Yanai, and T. Yasunari, 1998: Monsoons: Processes, predictability, and the prospects for prediction. *J. Geophys. Res.,* **103,** 14 451–14 510.

——, A. M. Moore, J. P. Loschnigg, and R. R. Leben, 1999: Coupled ocean–atmosphere dynamics in the Indian Ocean during 1997–98. *Nature,* **401,** 356–360.

Xie, P., and P. A. Arkin, 1996: Analyses of global monthly precipitation using gauge observations, satellite estimates, and numerical model predictions. *J. Climate,* **9,** 840–858.

Yang, S., K.-M. Lau, and M. Sankar-Rao, 1996: Precursory signals associated with the interannual variability of the Asian summer monsoon. *J. Climate,* **9,** 949–964.

Yasunari, T., 1990: Impact of Indian monsoon on the coupled atmosphere/ocean system in the tropical Pacific. *Meteor. Atmos. Phys.,* **44,** 29–41.

——, and Y. Seki, 1992: Role of the Asian monsoon on the interannual variability of the global climate system. *J. Meteor. Soc. Japan,* **70,** 177–189.